


Phase II study of ceralasertib (AZD6738) in combination with durvalumab in patients with advanced gastric cancer

Minsuk Kwon,^{1,2} Gahyun Kim,^{3,4} Ryul Kim,¹ Kyu-Tae Kim,⁵ Seung Tae Kim,¹ Simon Smith,⁶ Peter G S Mortimer,⁶ Jung Yong Hong,¹ Arsene-Bienvenu Loembé,⁶ Itziar Irurzun-Arana,⁶ Loumpiana Koulai,⁶ Kyoung-Mee Kim ,⁷ Won Ki Kang,¹ Emma Dean,⁶ Woong-Yang Park,⁸ Jeeyun Lee^{1,9}

To cite: Kwon M, Kim G, Kim R, *et al.* Phase II study of ceralasertib (AZD6738) in combination with durvalumab in patients with advanced gastric cancer. *Journal for ImmunoTherapy of Cancer* 2022;**10**:e005041. doi:10.1136/jitc-2022-005041

► Additional supplemental material is published online only. To view, please visit the journal online (<http://dx.doi.org/10.1136/jitc-2022-005041>).

MK and GK contributed equally.

Accepted 25 May 2022

ABSTRACT

Background Targeting the DNA damage repair (DDR) pathways is an attractive strategy for boosting cancer immunotherapy. Ceralasertib (AZD6738) is an oral kinase inhibitor of ataxia telangiectasia and Rad3 related protein, which is a master regulator of DDR. We conducted a phase II trial of ceralasertib plus durvalumab in patients with previously treated advanced gastric cancer (AGC) to demonstrate the safety, tolerability, and clinical activity of the combination.

Methods This phase II, open-label, single-center, non-randomized study was designed to evaluate the efficacy and safety of ceralasertib in combination with durvalumab in patients with AGC. The study drug regimen was ceralasertib (240 mg two times a day) days 15–28 in a 28-day cycle in combination with durvalumab (1500 mg) at day 1 every 4 weeks. The primary end point was overall response rate (ORR) by Response Evaluation Criteria in Solid Tumors (V.1.1). Exploratory biomarker analysis was performed using fresh tumor biopsies in all enrolled patients.

Results Among 31 patients, the ORR, disease control rate, median progression-free survival (PFS), and overall survival were 22.6% (95% CI 9.6% to 41.1%), 58.1% (95% CI 39.1% to 75.5%), 3.0 (95% CI 2.1 to 3.9) months, and 6.7 (95% CI 3.8 to 9.6) months, respectively. Common adverse events were manageable with dose modification. A subgroup of patients with a loss of ataxia telangiectasia mutated (ATM) expression and/or high proportion of mutational signature attributable to homologous repair deficiency (sig. HRD) demonstrated a significantly longer PFS than those with intact ATM and low sig. HRD (5.60 vs 1.65 months; HR 0.13, 95% CI 0.045 to 0.39; long-rank $p < 0.001$). During the study treatment, upregulation of the innate immune response by cytosolic DNA, activation of intratumoral lymphocytes, and expansion of circulating tumor-reactive CD8 + T cell clones were identified in responders. Enrichment of the tumor vasculature signature was associated with treatment resistance.

Conclusions Ceralasertib plus durvalumab has promising antitumor activity, with durable responses in patients with refractory AGC. Thus, a biomarker-driven trial is required.

Trial registration NCT03780608.

WHAT IS ALREADY KNOWN ON THIS TOPIC

⇒ Alterations in DNA damage repair (DDR) pathway of tumors are highly associated with the response of immune checkpoint inhibitors (ICI). Moreover, combination strategy of targeting DDR pathways with ICIs can be a promising approach to improve efficacies of ICIs.

WHAT THIS STUDY ADDS

⇒ Ceralasertib plus durvalumab displays a promising efficacy and manageable toxicity in patients with refractory advanced gastric cancer. Loss of ataxia telangiectasia mutated expression and/or high proportion of mutational signature related to homologous repair deficiency in tumor was related to favorable progression-free survival. Activations of innate and adaptive immune responses were identified in responders during treatment.

HOW THIS STUDY MIGHT AFFECT RESEARCH, PRACTICE OR POLICY

⇒ Further biomarker driven trial is warranted for ceralasertib plus durvalumab.

BACKGROUND

Systemic treatment options for advanced gastric cancer (AGC) have evolved rapidly in recent years. Central among these is the recent approval of immune checkpoint inhibitors (ICIs) as treatment for chemorefractory AGC, which has provided insight on immunotherapy for AGC.¹ The treatment paradigm for frontline treatment for AGC has changed following approval of anti-programmed cell death 1 (PD-1) agents in combination with conventional chemotherapy.^{2–4} The clinical benefit of ICIs was established in a subset of GC patients with high microsatellite instability, Epstein-Barr virus positivity, or high programmed death ligand 1 (PD-L1) expression.⁵ However, approximately 85% of patients experience primary resistance and minimal ICI benefit. Furthermore, patients



© Author(s) (or their employer(s)) 2022. Re-use permitted under CC BY-NC. No commercial re-use. See rights and permissions. Published by BMJ.

For numbered affiliations see end of article.

Correspondence to

Jeeyun Lee; jeeyunlee@skku.edu

who respond to ICIs often develop acquired resistance.⁶ However, limited treatment options exist once resistance develops, highlighting the need for further novel therapies or strategies that can increase the proportion of patients, including salvage patients with ICI resistance that can benefit from ICIs.

The recent approval of ICIs for tumors with defective mismatch repair has made it possible to investigate the role of DNA damage repair (DDR) defects in sensitizing cancer to ICI therapy.⁷ Alterations in DDR genes confer genomic instability in cancer cells, resulting in increased somatic mutations and neoantigen load.⁸ By promoting PD-L1 expression and tumor-infiltrating lymphocyte infiltration, genomic instability may enhance tumor immunogenicity and tumor microenvironment (TME),⁹ which are potential determinants of response to ICI treatment. Therefore, combination treatment of ICIs and DNA-damaging therapeutics could theoretically alleviate resistance and enhance efficacy of ICI treatment, as recently reported.¹⁰

Ataxia telangiectasia mutated (ATM) and ataxia telangiectasia and Rad3-related protein kinase (ATR) are essential components of DDR in human cells.¹¹ Ceralasertib (formerly AZD6738) is a potent, selective oral ATR inhibitor that suppresses the replication stress response induced by DNA damage in the S-phase of the cell cycle in tumor cells. Several studies demonstrated a promising antitumor activity of ceralasertib in combination with chemotherapy for treating refractory metastatic cancer.^{12–13} In addition, melanoma and non-small cell lung cancer patients who were previously treated with anti-PD1 agents showed favorable responses in a currently ongoing phase II clinical trial.^{14–15}

Here, we report the first phase II trial of ceralasertib plus durvalumab (ceralasertib +durvalumab), an anti-PD-L1 antibody, for AGC treatment. We demonstrated the safety, tolerability, and clinical activity of this combination in patients with chemorefractory AGC. Focusing on a subset of patients with adequate tissue specimens for sequencing, we attempted to identify potential biomarkers for the therapeutic efficacy of the combination treatment.

METHODS

Study design and participants

This was a phase II, open-label, single-center, non-randomized study conducted at the Samsung Medical Center (Seoul, Korea). The eligibility criteria were as follows: (1) histologically confirmed diagnosis of gastric or gastroesophageal junctional adenocarcinoma; (2) prior failure of at least one line of chemotherapy that included platinum/fluoropyrimidine; (3) at least 19 years of age; (4) at least one measurable lesion according to the Response Evaluation Criteria in Solid Tumors (RECIST) V.1.1; (5) adequate organ function per protocol; and (6) Eastern Cooperative Oncology Group performance

status 0 or 1. Patients with prior anti-PD-1 or anti-PD-L1 treatments were not excluded.

All patients received 1500 mg of intravenous durvalumab (MEDI-4736) infused over 60 min on day 1, followed by 240 mg of ceralasertib twice daily on days 15–28, until disease progression, unacceptable toxicity, or withdrawal of consent. The treatment cycle lasted for 4 weeks (online supplemental figure S1A). Dose reductions of durvalumab were not allowed but ceralasertib was dose-reduced to 160 mg two times per day and subsequently to 160 mg once daily for treatment-emergent AEs. Response was assessed every 2 months according to RECIST V.1.1. Adverse events (AEs) were summarized using the preferred terms, and graded according to the National Cancer Institute Common Terminology Criteria for AEs 5.0.

The primary endpoint was the objective response rate (ORR), according to RECIST V.1.1. The secondary endpoints included disease control rate (DCR), progression-free survival (PFS), overall survival (OS), safety, and exploratory biomarkers.

Tumor sample and peripheral blood collection

To explore potential biomarkers, primary gastric tumor tissues were obtained via endoscopic biopsy at any time from 1 to 28 days before commencing the study treatment. Matched peripheral blood (PB) samples were collected prior to treatment initiation. After two cycles of study treatment, blood and tissue samples were collected if available. If tumor cellularity was estimated to be >40% after a thorough pathological review, tumor DNA and RNA were extracted from freshly obtained tumor tissues using a QIAamp Mini Kit (Qiagen, Hilden, Germany) according to the manufacturer's instructions. RNaseA (cat. #19101; Qiagen) was used for RNase digestion during the DNA preparation. We measured the concentrations and 260/280 and 260/230 nm absorption ratios using a NanoDrop 1000 Spectrophotometer (NanoDrop Technologies LLC, Thermo Fisher Scientific, Massachusetts, USA), while DNA/RNA was quantified using a Qubit Fluorometer (Life Technologies, California, USA).

Immunohistochemistry for ATM and PD-L1

Immunohistochemistry (IHC) was performed using an automatic immunostainer (Dako, Glostrup, Denmark) according to the manufacturer's instructions. To assess ATM protein expression by IHC, a primary anti-ATM antibody was used (Y170; Abcam Plc., Cambridge, UK). Regardless of the cytoplasmic staining status, cancer cells showing nuclear staining were considered positive for ATM. Loss of ATM protein expression was defined as nuclear expression in ≤20% of the stained cells as previously reported.¹⁶ For PD-L1 IHC, we used Dako PD-L1 IHC 22C3 pharmDx kit (Agilent Technologies, California, USA) with the EnVision FLEX visualization system (Agilent Technologies) and counterstained with hematoxylin according to the manufacturer's instructions. PD-L1 protein expression was assessed using the Combined

Positive Score (CPS), which refers to the percentage of PD-L1-stained cells (tumor cells, lymphocytes, and macrophages) among viable tumor cells. Specimen was considered PD-L1-positive when CPS was ≥ 1 .

Whole-exome sequencing, whole-transcriptome sequencing, single-cell RNA-seq, and data processing

The detailed process of library preparation and data analysis in whole-exome sequencing (WES), whole-transcriptome sequencing (WTS), and single-cell RNA sequencing are described in online supplemental methods.

Sample size and statistical analysis

The planned sample size was calculated according to Simon's two-stage minimax design, assuming 90% power, hypothesis rejected at $RR < 15\%$, a one-sided alpha level of 5%, assuming expected ORR of 40%, and 10% non-response rate. The total number of patients available for evaluation was 27 and 30 patients were recruited to reflect a 10% drop-off rate. In the first stage, if there were fewer than two responses from the initial 16 patients, the study was stopped. Statistical associations between continuous variables were evaluated using Spearman's correlations, and those between continuous and categorical variables were evaluated using rank-sum statistics. The non-parametric Mann-Whitney U-test was used to compare between two groups with non-normally distributed data. Paired values were compared using non-parametric Wilcoxon matched-pair signed-rank test. Survival analyses were performed using the Kaplan-Meier method, and differences were analyzed using the log-rank test. HRs and corresponding 95% CIs were calculated using the Cox proportional hazards model. PFS was defined as the time from treatment initiation to date of disease progression or death from any cause. OS was defined from treatment initiation to date of death from any cause. Among patients receiving at least one dose of ceralasertib and durvalumab, ORR was defined as the proportion of patients who experienced complete response (CR) or partial response (PR) and DCR (defined as the proportion of patients presenting with CR, PR, or stable disease (SD)). All statistical analyses were performed using R V.3.6.0 (<http://www.r-project.org>) or Prism (V.8.4; GraphPad, Waltham, Massachusetts, USA). The data cut-off date was December 11, 2020.

RESULTS

Anti-tumor activity of the study treatment

This study enrolled 31 patients with AGC between August 2019 and March 2020. Baseline demographic and disease characteristics are shown in [table 1](#). At data cut-off date, RECIST response evaluations were available for 30 patients, with a median follow-up of 14.1 (range 8.8–16.7) months. One patient (ID16) who developed ischemic stroke after one study treatment cycle progressed and died before response evaluation. Seven patients (22.6%)

Table 1 Patient characteristics

Characteristics	Values*
Age, median (range)	55 (39–74)
Gender	
Male	23 (74.2)
Female	8 (25.8)
Previous gastrectomy	
Yes	5 (16.1)
No	26 (83.9)
Primary tumor site	
Cardia	1 (3.2)
Body	13 (41.9)
Angle	13 (41.9)
Antrum	4 (12.9)
Metastatic site	
Liver	10 (32.3)
Lung	2 (6.5)
Lymph nodes	28 (90.3)
Peritoneum	18 (58.1)
Prior lines of chemotherapy	
1 regimen	15 (48.4)
2 regimens	11 (35.5)
≥ 3 regimens	5 (16.1)
Prior anti-PD1 therapy	2 (6.5)
Prior HER-2 directed therapy	2 (6.5)
Pathology	
Poorly differentiated	13 (41.9)
Moderately differentiated	12 (38.7)
Signet ring cell carcinoma	6 (19.4)
HER2 positive	2 (6.5)
EBV positivity	
Positive	5 (16.1)
Negative	23 (74.2)
Not available	3 (9.7)
PD-L1 (22C3)	
Positive	24 (77.4)
Negative	5 (16.1)
Not available	2 (6.5)
ATM IHC	
Loss	8 (25.8)
Intact	21 (67.7)
Not available	2 (6.5)
Mismatch repair	
Microsatellite stable	30 (96.8)
Microsatellite instability-high	1 (3.2)

*Number (%) if not specified.

ATM, ataxia telangiectasia mutated; EBV, Epstein-Barr virus; IHC, immunohistochemistry.

achieved PR (3 (42.9%) and maintained the response for >6 months (median duration, 5.7 (95% CI, 4.9 to 6.5) months; (figure 1B)); 11 (35.5%) achieved SD with ORR of 22.6% (95% CI 9.6 to 41.1) and DCR of 58.1% (95% CI 39.1% to 75.5%) (figure 1A, online supplemental table S1). Notably, two patients (ID01, SD in prior nivolumab; ID05, PR in prior pembrolizumab +XELOX) who progressed on prior-anti-PD1 treatment demonstrated PR (ID01) or SD (ID05) (figure 1B). Twenty-four patients (77.4%) had PDL1-expressing tumors (table 1) of which 6 (25%) had a PR while one of five patients with a PDL1-negative tumor had a RECIST PR (20%) (online supplemental table S2). Tumors with loss of ATM expression were enriched in patients with the best response (SD or PR) (figure 1B). Specifically, half of the patients with ATM loss responded to treatment; 14.3% with intact ATM had a PR (online supplemental table S2). At data cut-off date, 30 PFS events (median, 3.0 (95% CI 2.1 to 3.9 months)) occurred (figure 1C), and 26 patients died (median OS, 6.7 (95% CI 3.8 to 9.6) months) (figure 1D).

Safety profile

Among 31 patients who received ≥ 1 dose of both ceralasertib and durvalumab, treatment-emergent AEs of any grade occurred in 30 (96.8%) patients; the most common AEs were fatigue, nausea, anorexia, anemia, thrombocytopenia, and vomiting (table 2). Twenty-three (74%) patients reported grades 3 or 4 treatment-emergent AEs, mostly of hematologic origin (anemia (n=11, 35.5%), thrombocytopenia (n=11, 35.5%), and neutropenia (n=2, 6.7%)), which are expected toxicities of ceralasertib. All grade ≥ 3 AEs improved following drug administration interruptions and supportive care, including intermittent transfusions. No treatment-related deaths occurred during this period. Ceralasertib dose reduction following treatment-emergent AEs occurred in 15 (48.4%) patients (240 mg two times per day to 160 mg two times per day (9 patients) or to 160 mg every day (6 patients) for 14 days, respectively) commonly due to thrombocytopenia (grade ≥ 3) and neutropenia (grade ≥ 3). None of the patients discontinued durvalumab or ceralasertib owing to AEs.

Responders genomic characterization

To explore the molecular characteristics of AGC in response to ceralasertib plus durvalumab, we investigated whole-exome sequences of pretreatment biopsy specimens. Overall, 24 tumors with matched blood samples were available for WES (online supplemental figure S1B). We analyzed WES sequences in a unified pipeline (mean sequencing coverages of $\sim 200\times$ for tumor and matched blood samples) and mapped out the mutational landscape between responders and non-responders, focusing on consensus cancer driver genes¹⁷ and DDR pathway¹⁸ (figure 2A). Samples displayed a variable tumor mutational burden (TMB; median, 2.90 (range, 0.53–12.62)) mutations per megabase (figure 2A, upper). TMB tended to be higher in responders than in those without a RECIST

response, whereas tumors from patients with PD had a significantly lower TMB than those with PR ($p=0.018$, Mann-Whitney-U test; figure 2B). Notably, mutations of genes involved in DDR were significantly enriched in partial responders ($p=0.022$, Mann-Whitney-U test; figure 2A).

Loss of ATM expression was exclusively found in patients with PR or SD, in addition to one patient with mismatch repair-deficient tumors (ID26) (figures 1B and 2A). Furthermore, patients with ATM loss and/or mutations attributable to homologous recombination deficiency tended to benefit from study treatment (10/11 with HR deficiency had best responses of PR or SD vs 3/13 with HR proficiency) (figure 2A,C), while those with HR deficiency had significantly superior PFS (HR 0.13, 95% CI 0.045 to 0.39, $p=0.0002$; figure 2D). Multivariate analysis identified ATM loss and/or high signature attributable to homologous repair deficiency (sig. HRD) as the single most significant factor predicting favorable PFS in AGC patients treated with ceralasertib plus durvalumab (figure 2e). Patient ID24, a male patient (66 years old) with AGC and loss of ATM expression had a high sig.HRD and frequent copy number alterations (online supplemental figure S2A). This patient progressed on frontline treatment with 5-fluorouracil and oxaliplatin. After two cycles of ceralasertib plus durvalumab, metastatic liver lesions markedly decreased, and the patient remained on treatment for >12 months. In contrast, patient ID02 (56 years old, male) with HR-proficient disease, rapidly progressed after two cycles of study treatment (online supplemental figure S2B). The tumor of patient ID02 had intact ATM expression and low sig.HRD and was genomically stable.

Evolving TME during treatment with ceralasertib+durvalumab

We performed pretreatment WES and WTS and collected on-treatment biopsy samples to examine the effect of ceralasertib plus durvalumab on AGC and its TME. While TMB per se did not change significantly during the study treatment, responders had an increased proportion of neoantigens in the on-treatment samples ($p=0.024$, figure 3A). Gene set variation analysis identified significant upregulation of innate immune responses to cytosolic DNA and enriched signatures related to T and B lymphocyte activation during the study treatment in responders compared with those in non-responders (figure 3B, online supplemental figure S3A). By deconvoluting the expression profiles of WTS data, we estimated TME cellular proportions, revealing increased cytotoxic T lymphocytes in responders on study treatment ($p=0.142$, online supplemental figure S3B). Collectively, these results revealed the remodeling of TME, favoring T cell activation in patients who responded to ceralasertib plus durvalumab.

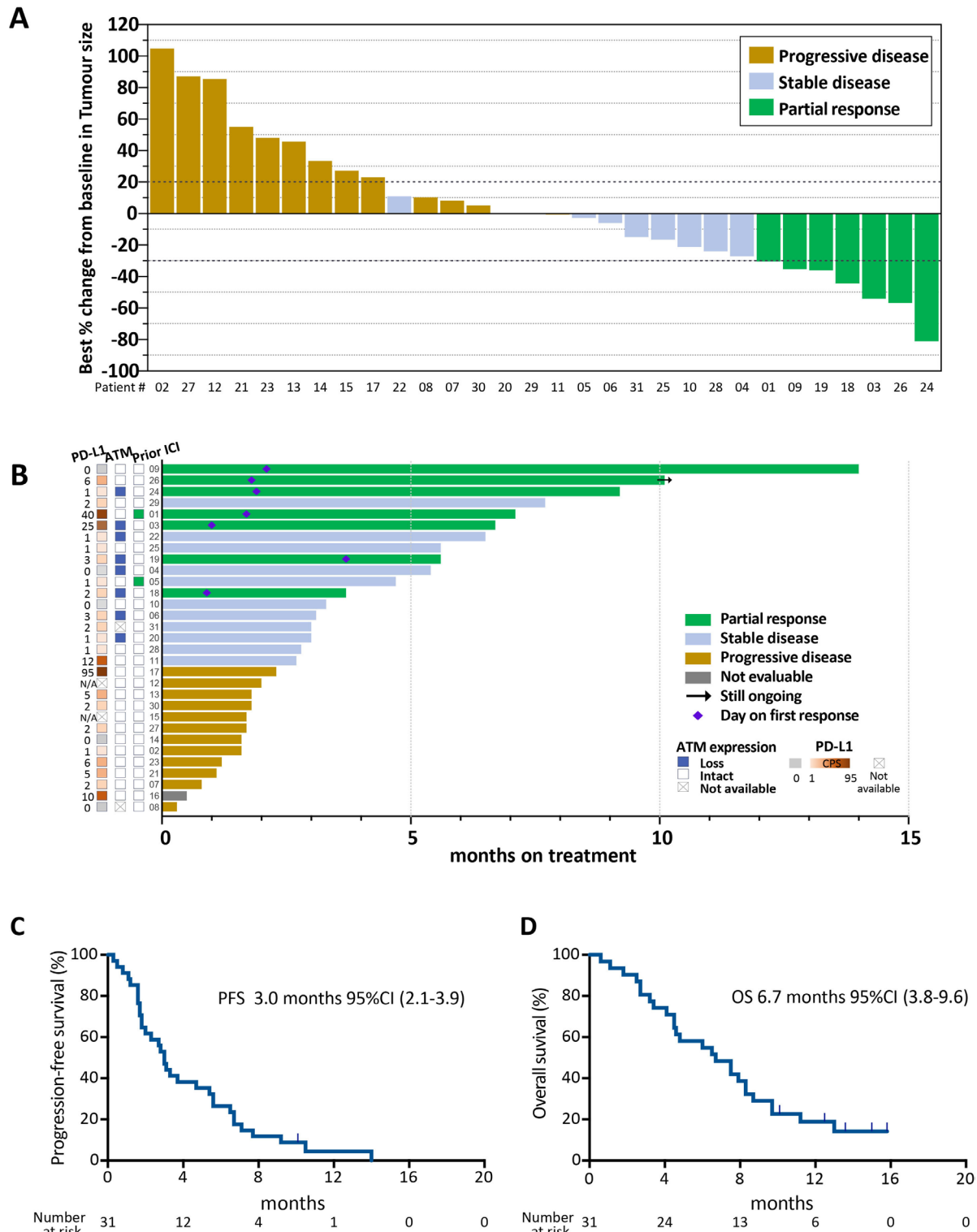


Figure 1 Response to ceralasertib in combination with durvalumab (A) A waterfall plot of best response to ceralasertib in combination with durvalumab in patients with advanced gastric cancer. The y-axis represents the percentage of maximum tumor reduction assessed according to RECIST V.1.1. Among 31 participants, overall, 30 were eligible for this analysis, because one patient (ID16) died from ischemic stroke before response evaluation. The upper and lower dotted lines represent 20% tumor growth and 30% tumor reduction, respectively, which define progressive disease and partial response. (B) A swimmer plot demonstrating the clinical courses of study participants. The left panel shows the expression of PD-L1 and ATM, and responses to prior immunotherapy. White blocks with a cross indicate unavailable data; white blocks in the prior ICI column indicate no prior ICI treatment. The diamond-shaped points indicate the time from study enrollment to the detection of the first response. Patients who were on study treatment at the cut-off date are marked by arrows heading to the right. (C, D) Kaplan-Meier curves of PFS and OS among the enrolled patients. N/A, not available; PFS, progression-free survival; RECIST, Response Evaluation Criteria in Solid Tumors; OS, overall survival.

Table 2 Treatment-emergent adverse events occurring in >3% of patients in the safety analysis set by CTCAE grade

	Any grade (%)	Grade 3 (%)	Grade 4 (%)
Patients with any AE	30 (96.8)	15 (48.4)	8 (25.8)
Fatigue	22 (71.0)		
Nausea	20 (64.5)		
Anorexia	19 (61.3)		
Anemia	16 (51.6)	9 (29.0)	2 (6.5)
Thrombocytopenia	15 (48.4)	6 (19.4)	5 (16.1)
Vomiting	13 (41.9)		
Abdominal pain	7 (35.5)		
Pruritus	7 (22.6)		
Neutropenia	6 (19.4)	2 (6.5)	
Ascites	5 (16.1)		
Non-neutropenic fever	4 (12.9)		
Dyspepsia	4 (12.9)		
Headache	4 (12.9)		
AE, adverse event; CTCAE, Common Terminology Criteria for Adverse Event.			

Increased tumor-reactive CD8⁺ T cell clones in PB during treatment with ceralasertib plus durvalumab

To investigate the immunologic phenotype associated with ceralasertib plus durvalumab response, we performed single-cell RNA sequencing and T-cell receptor (TCR) sequencing of PB samples from eight selected patients (figure 4A, online supplemental figure S4). After unsupervised clustering, we annotated each cell cluster according to canonical immune cell markers and identified four major immune cell types and various immune cell subtypes (T cells (n=11 460); NK cells (n=8161); myeloid cells (n=10 744); B cells (n=1143); and platelets (n=301)) (online supplemental figures S4–S6).¹⁹ We noted distinct immune cell composition in pretreatment blood samples between responders and progressors (ie, those with a best PD response) (figure 4B, online supplemental figure S4B–D). Specifically, progressors had a higher CD4⁺, CD8⁺, and $\gamma\delta$ T cells in pretreatment PB samples, while NK cells were enriched in responders. During the study, we observed increased T cell proportions in both responders and progressors (figure 4C). However, TCR clonality demonstrated variable changes during treatment in responders, while progressors had decreased TCR clonality in on-treatment samples compared with that in pretreatment samples (figure 4D). To analyze the dynamic changes in PB CD8⁺ T cells that are crucial for cytotoxicity against cancer cells during the study treatment, we compared TCR clonal frequencies of PB CD8⁺ T cells between pretreatment and on-treatment. We also annotated each clone as persistent, expanded, contracted, and novel T cell clone (figure 4E).²⁰ Interestingly, patients with PR had significantly higher frequencies

of novel or expanded PB CD8⁺ T cell clones during study treatment than did patients with PD (p=0.002, figure 4F). We found that the novel or expanded PB CD8⁺ T cell clones from the patients with PR expressed high levels of PD-1 (*PDCD1*), *TIGIT*, CTLA-4 (*CTLA4*), *TOX*, CD103 (*ITGAE*), and *CD69*, implying tumor-reactive T cells circulating in PB during study treatment (figure 4G).²¹ To delineate whether novel or expanded PB CD8⁺ T cell clones from patients with PR were relevant to tumor-reactive T cells, we estimated the binding affinity between TCR of the novel or expanded PB CD8⁺ T cells and major histocompatibility complex (MHC)-neoantigen peptide that newly occurred on-treatment in each patient. The estimated binding affinity score was significantly higher in patients with PR than in those with PD (figure 4H). Altogether, these data suggest that circulating tumor-reactive CD8⁺ T cell clones increased in response to ceralasertib plus durvalumab.

Enriched tumor vasculature and treatment resistance with ceralasertib+durvalumab

To explore the molecular characteristics of the TME, including resistance, we analyzed the pre-treatment WTS data of non-responders and responders. Overall, 193 differentially expressed genes were identified between non-responders and responders. In gene-set enrichment analysis, several canonical pathways involved in angiogenesis were commonly enriched in non-responders, including hepatocyte growth factor (p=0.001), vascular endothelial-derived growth factor (p=0.007), interleukin 6 (p=0.003), and platelet-derived growth factor (p<0.001) (figure 5A). Moreover, genes involved in DDR, metastasis, angiogenesis, wound healing, and hypoxia were significantly upregulated in progressors (figure 5B). As with gene set enrichment analysis, deconvoluting WTS data also revealed higher abundance of endothelial cells in progressors (figure 5C). In brief, enriched angiogenesis signature in TME was associated with resistance to the study treatments.

Considering how the TME is related to more comprehensive ICI responses, we classified each pretreatment sample into four distinct microenvironment subtypes (immune-depleted, fibrotic, immune-enriched, and immune-enriched/fibrotic) to predict immunotherapy response (figure 5D).²² Overall, this subtyping did not predict study treatment response. All patients with immune-enriched/fibrotic subtype showing enriched angiogenesis signature did not demonstrate response to ceralasertib plus durvalumab, while patient ID03 with fibrotic subtype who showed a low angiogenesis and high T cell traffic signature demonstrated PR to ceralasertib plus durvalumab (figure 5D,E). In addition, among the 29 genes that determine the four distinct microenvironment subtypes, a lower level of T cell trafficking was identified in progressors than in responders (figure 5F). In brief, an enriched tumor vascular signature in TME before the study treatment was associated with a poor response to ceralasertib plus durvalumab.

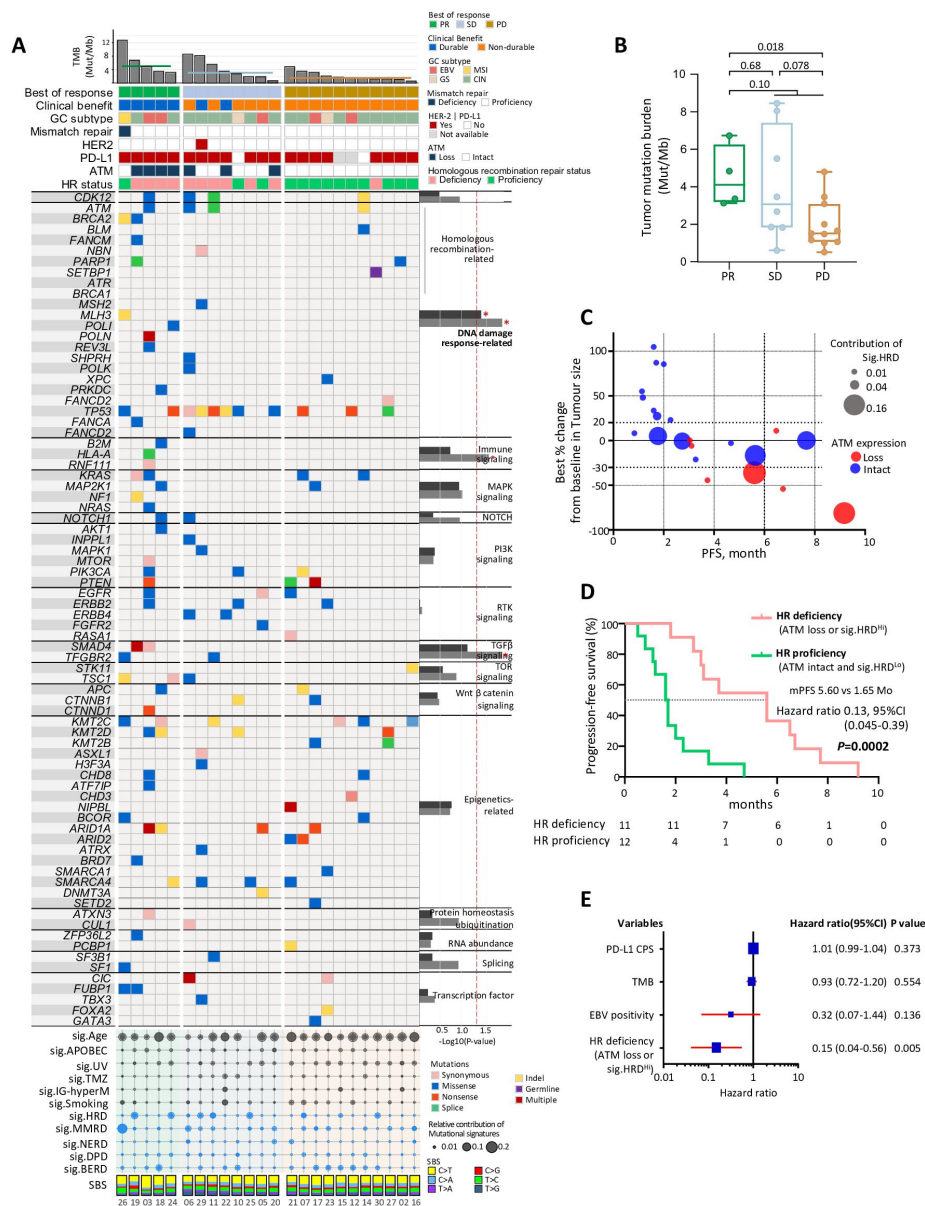


Figure 2 Exploratory biomarker analysis. (A) Landscape of genetic alterations in study samples obtained from 24 patients with advanced gastric cancer (AGC). Top to bottom: non-synonymous tumor mutational burden (TMB) in the exome, response to the study treatment, durability of clinical response, subtype of gastric cancer defined by The Cancer Genome Atlas (TCGA),⁴¹ microsatellite stability, HER2 expression, PD-L1 positivity, ATM expression, homologous recombination repair status, somatic nucleotide variations in selected canonical oncogenes and tumor suppressor genes, mutational signatures of somatic mutations, and the proportion of single base substitution subtypes in each sample. Response was defined to be durable if treatment duration was more than 6 months. Samples with ATM loss and/or high HRD signature were considered to have deficient homologous recombination repair. We assessed the enrichment of mutation groups in responders or non-responders using two-tailed Student's t-test. Genes are grouped by pathway or function.^{42 43} The corresponding log-transformed p values are illustrated on the right with bar plots: Black bars represent comparison of responders (PR) and progressors (SD, PD) and gray bars represent comparison of PR and PD. Significantly enriched mutation groups in responders are marked by asterisks (*). (B) The exonic tumor mutational burden in patients with PR, SD, and PD to the study treatment. The statistical significance of the differences was estimated by the Wilcoxon signed-rank test. (C) A scatter plot simultaneously demonstrating the PFS, x-axis, best response from baseline in tumor size (y-axis), ATM expression (color), and proportion of mutational signature attributable to deficient HRD signature, size). (D) Kaplan-Meier plots of PFS among study patients according to ATM expression and proportion of HRD signature. Samples with HRD signature proportion higher than the average were defined as those with high proportion of HRD signature (sig. HRD^{Hi}). (E) A forest plot demonstrating multivariate analysis of factors associated with PFS. HRs and corresponding p values were estimated using multivariate cox regression hazard model. CIN, chromosomal instability; CPS, combined positive score; GS, genomically stable; HR, homologous recombination; HRD, homologous recombination deficiency; mPFS, median progression-free survival; MSI, microsatellite instability; PD, progressive disease; PFS, progression-free survival; PR, partial response; SBS, single-base substitution; SD, stable disease; TMB, tumor mutational burden.



Figure 3 Evolving tumor microenvironment during treatment with ceralasertib plus durvalumab. (A) Changes in TMB and neoantigen ratio (the number of neoantigen divided by the total sum of mutation count) during the study treatment. Changes during treatment were calculated by subtracting TMB or neoantigen ratio of pre-treatment from that of on-treatment. The statistical significance of the differences was estimated by the Wilcoxon signed-rank test. (B) A heatmap illustrating changes in single-sample gene set enrichment analysis (ssGSEA) scores of significant pathways during the study treatment. The ssGSEA scores were obtained from whole transcriptome sequencing (WTS) data from pretreatment and on-treatment samples of eight study participants, and we calculated the changes by subtracting the ssGSEA score of pretreatment from that of on-treatment. The statistical significance was estimated via Wilcoxon rank-sum test. PD, progressive disease; PR, partial response; SD, stable disease; TMB, tumor mutational burden.

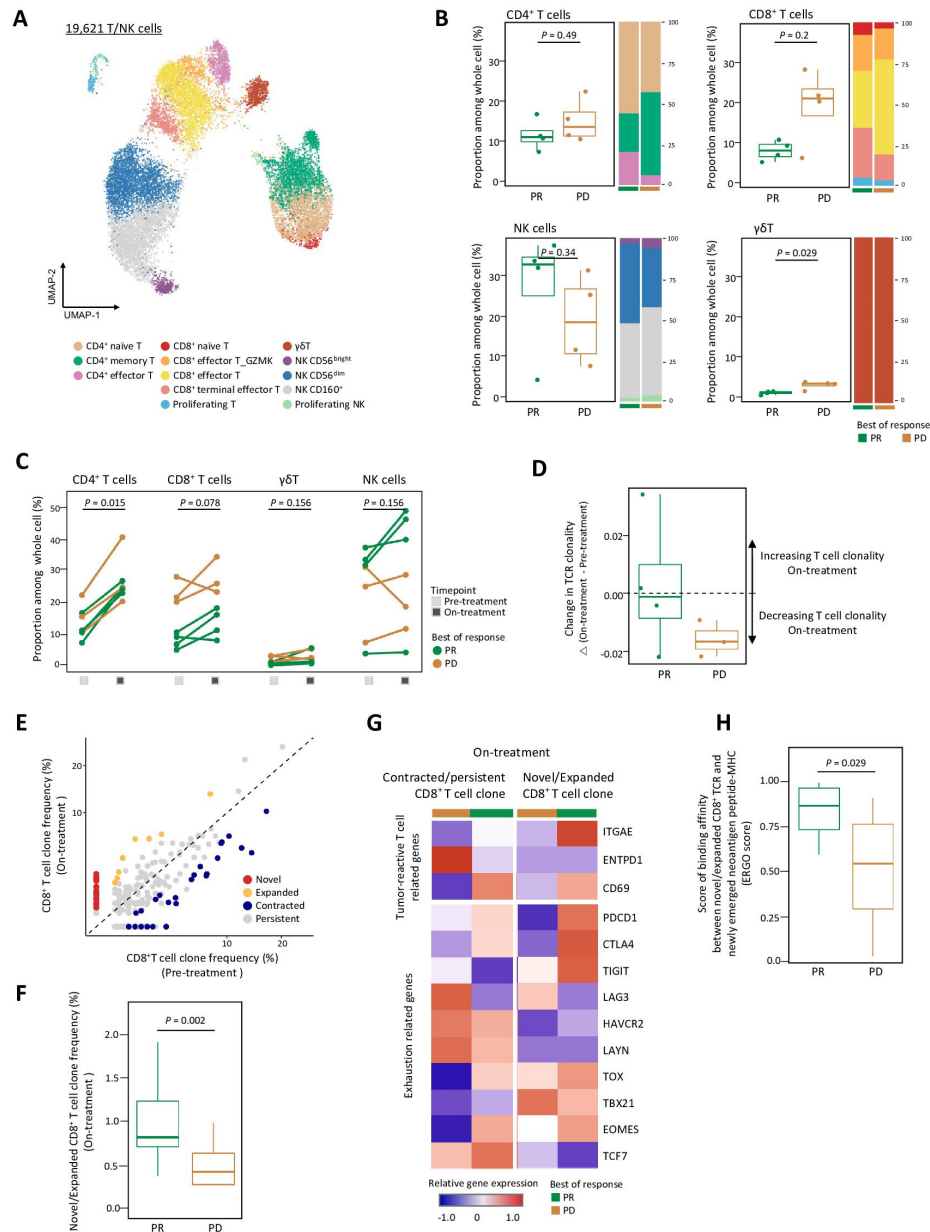


Figure 4 Association of cellular composition of peripheral blood mononuclear cells with ceralasertib plus durvalumab response. We performed single-cell RNA sequencing and T cell receptor (TCR) sequencing on peripheral blood samples from eight patients. (A) Uniform manifold approximation and projection (UMAP) visualization of 19,621 cells in the T cell and NK cell lineage from pretreatment (n=8) and on-treatment (n=7) peripheral blood samples. (B) Proportion of T/NK cells in pretreatment peripheral blood samples. Box plots show the difference in proportion of T/NK cell subtypes, which are categorized into CD4⁺ T cells, CD8⁺ T cells, NK cells, and $\gamma\delta$ T cells, between responders (partial response, n=4) and progressors (progressive disease, n=4). The p values were estimated by Wilcoxon rank sum test. The stacked bar plots to the right of each box plot show the relative proportions of more subdivided cell types. (C) Change in the proportion of T/NK sub-cell types in peripheral blood during treatment. The p values from paired Wilcoxon signed-rank test are shown. (D) Change in the clonality of TCR repertoire during treatment. The change is calculated by subtracting TCR clonality of pretreatment from that of on-treatment. (E) Scatterplot of CD8⁺ T cell clone (n=1380 clones) frequencies of pretreatment and on-treatment. CD8⁺ T cell clones were categorized into four groups based on the Fisher's exact test. CD8⁺ T cell clones, which were newly detected on-treatment, were defined as novel clones (red). CD8⁺ T cell clones that significantly expanded after treatment were defined as expanded clones (yellow). CD8⁺ T cell clones that significantly contracted after treatment were defined as contracted clones (blue). The rest of the clones were defined as persistent clones (gray). (F) Box plot comparing frequencies of novel and expanded CD8⁺ T cell clones at on-treatment timepoint. The p values were estimated by Wilcoxon rank sum test. (G) Heatmap showing expression levels of genes known to be highly expressed in tumor-specific T cells at on-treatment timepoint in PR patients (n=4) and PD patients (n=3). (H) Box plot for comparing binding affinity score of PR (n=2) and PD (n=1) suitable for this analysis. The affinity score was estimated between newly emerged neo-peptides presented by MHC (pMHC) and novel or expanded CD8⁺ TCRs by ergo II.³⁸ The p values of Wilcoxon rank sum test are shown. All box plots describe the median and IQR. MHC, major histocompatibility complex; TCR, T cell receptor.

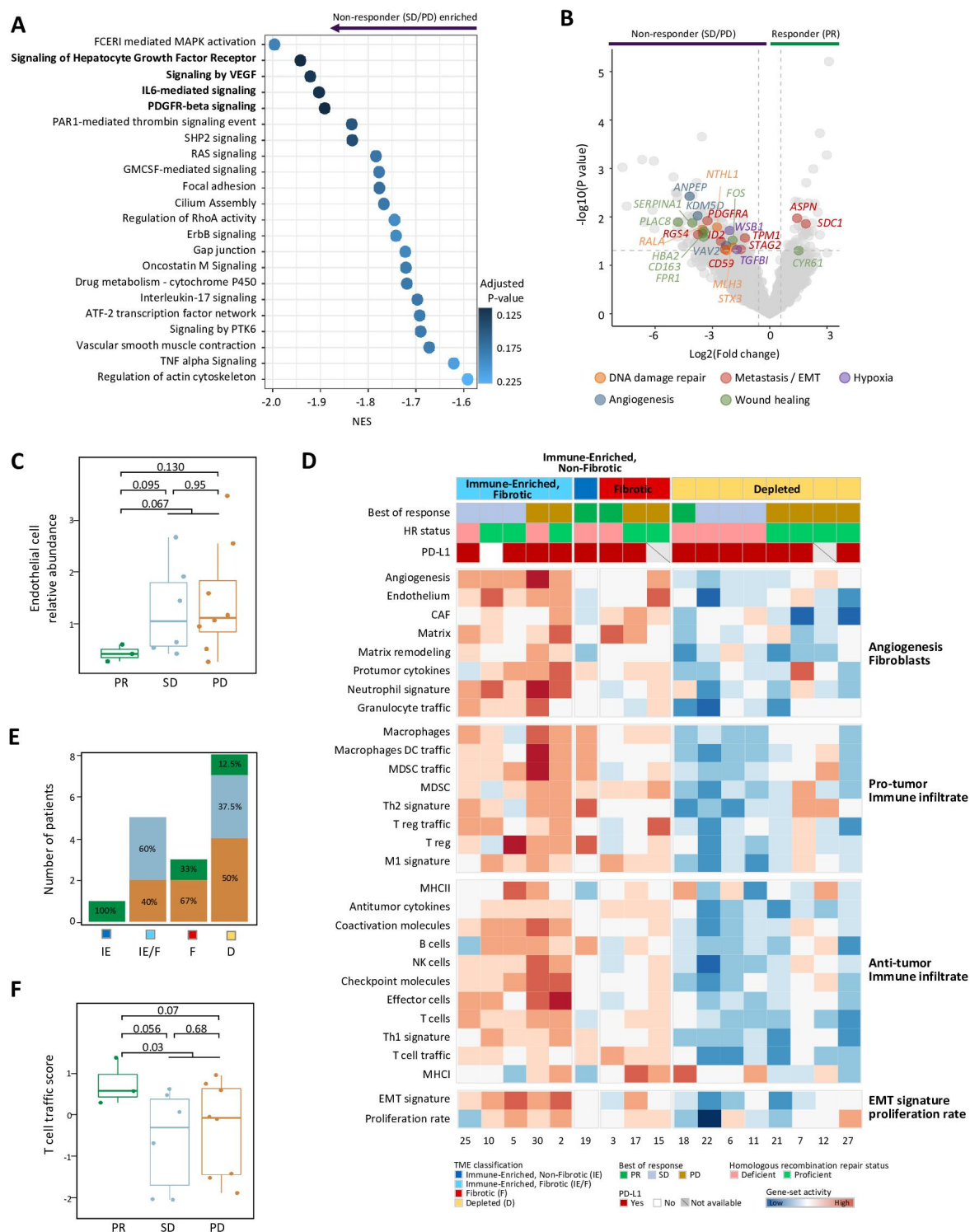


Figure 5 Tumor microenvironment associated with response to ceralasertib in combination with durvalumab (A) Dot plot showing enriched pathways in pre-treatment samples of non-responders compared to those of progressors. Threshold for selection was $FDR < 0.25$. The gene sets are ordered by normalized enrichment score (NES). The adjusted p value estimates the statistical significance of the enrichment score for multiple gene sets. (B) Volcano plot showing differentially expressed genes (DEGs) between responders and progressors before treatment, with gray dotted lines representing the selection criteria: log 2 fold change of mean expression $> |0.5|$; p value from Wilcoxon rank sum test < 0.05 . Principally, DEGs are categorized into five groups: DNA damage repair, Metastasis/EMT, Hypoxia, angiogenesis, and Wound healing. (C) Comparison of relative abundance of endothelial cells estimated with RNA-seq deconvolution analysis. (D) Heatmap showing 29 functional gene expression signatures (Fges) characterizing 4 TME subtypes. (E) Number of partial response (PR), stable disease (SD), and progressive disease (PD) patients across the TME subtypes. (F) Box plot of T cell traffic score, one of the Fges, being significantly associated with drug response. All box plots describe the median and IQR. The p values of Wilcoxon rank sum test are shown.

DISCUSSION

Recently, various combination strategies with anti-PD-(L) 1 have been investigated for metastatic GC, especially with the US Food and Drug Administration approval of chemotherapy plus nivolumab as first-line treatment. Treatment options need to be optimized for different subsets of patients with GC, preferably based on tumor characteristics. In this phase II trial, we investigated the combination of durvalumab and ceralasertib in refractory AGC patients, predominantly those with microsatellite stability (MSS). Ceralasertib plus durvalumab resulted in an ORR of 22.6% (7/31). Compared with previous response rates (0%–12%) in phase III trials of anti-PD(L)–1 monotherapy in different settings,^{2 23–25} the ORR achieved with this novel combination is promising.

Considering that chemotherapy plus IO is recommended as a first-line therapy for AGC, treatment options for patients with acquired resistance to IO therapy are needed. In this study, two patients with prior anti-PD-1 treatment had progressive disease before commencing this study treatment and did not receive intervening chemotherapy following anti-PD1 therapy. A patient (ID01) who received nivolumab and demonstrated SD as the best response had a PR to ceralasertib plus durvalumab. Patient ID05 received pembrolizumab +XELOX, demonstrated PR, and had SD as best study treatment response. Considering that ceralasertib plus durvalumab was active (ORR 31.0%) in metastatic melanoma after failure of prior anti-PD-1 therapy,¹⁵ ceralasertib plus durvalumab could be a promising strategy for AGC patients who fail prior IO or chemotherapy plus IO and is suitable as a salvage therapy.

Approximately 10%–20% of GC patients have pathogenic alterations in DDR family genes or complete ATM loss.^{26 27} In the prespecified biomarker analyses, ATM loss by IHC was associated with response to ceralasertib plus durvalumab (4 PR among 8 patients with ATM loss) in this trial. One possibility is to include ATM IHC to select patients with ATM protein loss in a larger prospective trial to validate our observation.

DDR signaling and repair is a complex, multi-step process involving multiple proteins including ch as breast cancer gene 1 (BRCA1), breast cancer gene 2 (BRCA2), ATM, ATR, RAD51 recombinase, and partner and localizer of BRCA2 (PALB2).²⁸ Mutation of the above genes may confer HRD, and assays that combine *BRCA* mutation status with ‘genomic scar,’ which is a pattern of accumulated somatic alterations caused by HRD, are used as companion diagnostics for Poly-ADP ribose (PARP) inhibitors in ovarian cancer (Myriad MyChoice and FoundationOne CDx).^{29 30} Although ATM is a vital component in HR repair (HRR), the proficiency of HRR is determined by the status of many factors in the pathway as well as ATM.³¹ Given the complexity, we examined both ATM protein loss and mutational signatures as indicators of defects in HR (single base substitution 3)³² and as predictors of study treatment response. In our data, patients whose tumors had a combination of ATM protein loss

and/or high sig.HRD score demonstrated significantly longer mPFS to ceralasertib plus durvalumab than those without (HR proficient group). Although mutational signatures reflect historical endogenous (DNA damage, repair and replication) and exogenous mutational processes,³² and correlate with clinical features such as survival and platinum-based chemotherapy response,^{33–37} hitherto mutational signatures have not been widely used as a predictive biomarker for DDR targeting agents. The major hurdle is the reliance on fresh-frozen tissues while most clinical samples are formalin-fixed. Considering the feasibility of sampling, ATM IHC and/or HRD assays that use formalin fixed tissues could be a practical alternative for large-scale clinical trials.

In exploratory analysis, we counted neoantigens per tumor mutation ratio by estimating the binding affinity between neopeptide sequence in tumor samples and HLA alleles per patient. Patients who demonstrated PR as their best response in the HR-deficient group showed significantly increased neoantigen ratio and increased transcriptomic signature of an innate immune response to cytosolic DNA, the so-called cyclic GMP-AMP synthase-stimulator of interferon genes (cGAS-STING) pathway³⁴ (figure 3A,B). Although limited by a small sample size, these data support the hypothesis that ATR inhibition could induce genomic instability in HR-deficient tumors and increase mutations, facilitating subsequent immune activation. The dynamic immune activation in the tumor immune microenvironment during study treatment might explain why PD-L1 expression in pre-treatment samples was not associated with clinical response.

Beyond HR deficiency, we analyzed dynamic changes in gene expression using tumor WTS and sc-RNA sequencing of PB obtained at baseline and during treatment. Along with the enriched signature of innate responses to cytosolic DNA, signatures of increased adaptive immune responses, such as B cell receptor, interleukin-2, and T cell receptor signaling, were identified in tumor tissues of patients with objective response. Furthermore, increased cytotoxic CD8⁺ T cells in tumor tissue and expanded tumor-reactive CD8⁺ T cells in PB were identified in patients with PR during study treatment. In contrast to the increase in T cell populations in the blood of all patients, novel or expanded CD8⁺ T cell clone frequencies were significantly higher in patients with PR than in those with SD or PD. Moreover, these novel or expanded T cells presented high levels of CD39, CD103, CD69, PD-1, TIGIT, and CTLA-4, which are markers of tissue-resident and tumor antigen-specific T cells.³⁸ The novel or expanded T cells had TCR sequences, predicted to have high affinity for the neoantigen peptide-MHC complex. Although our data were limited to TCR sequence data in PB, Wu *et al* reported that identifying clonal expansion in peripheral T cells can predict intratumoral T cell infiltration and clinical response to ICIs.³⁹ Collectively, these data suggest that ceralasertib plus durvalumab can show anti-tumor activity by reinvigorating exhausted T cells.

As tumor vasculature is known to promote immune suppression by hindering immune cell infiltration,⁴⁰ upregulated angiogenesis signatures and diminished T cell traffic features were identified in non-responders to ceralasertib plus durvalumab. Patient ID-30 who had HR-deficient tumor but showed disease progression demonstrated an enriched angiogenesis signature in the tumor before treatment (online supplemental figure S7D). Adding an anti-angiogenic agent might be an alternative strategy to overcome immune evasion in selected cases.

In conclusion, our study demonstrated that ceralasertib plus durvalumab was tolerable and led to an impressive ORR (22.6%) in a large MSS cohort of otherwise unselected metastatic GC patients with persistent or recurrent disease after previous chemotherapy. In this population, the clinical activity of single-agent PD-1 therapy is limited and the combination of ceralasertib plus durvalumab can be a potential treatment option for AGC patients, after failure of chemotherapy plus IO. The other treatment options here remain paclitaxel±ramucirumab and TAS-102, the latter of which is approved in the USA in patients who have received at least two prior lines of chemotherapy. Ceralasertib plus durvalumab is a potential future non-chemotherapy option. Our exploratory biomarker analysis suggested that AGC patients with either ATM loss and/or high HRD scores are especially likely to benefit from ceralasertib combination therapy. Biomarker enrichment strategies may be required to select patients who are most likely to benefit in future studies.

Author affiliations

¹Division of Hematology-Oncology, Department of Medicine, Samsung Medical Center, Sungkyunkwan University School of Medicine, Seoul, Republic of Korea

²Department of Hematology-Oncology, Ajou University, Suwon, Republic of Korea

³Samsung Advanced Institute of Health Science and Technology, Sungkyunkwan University, Seoul, Republic of Korea

⁴Samsung Genome Institute, Samsung Medical Center, Seoul, Republic of Korea

⁵Department of Physiology, Ajou University, Suwon, Republic of Korea

⁶Oncology R&D, AstraZeneca, Cambridge, UK

⁷Department of Pathology and Translational Genomics, Samsung Medical Center, Sungkyunkwan University School of Medicine, Seoul, Republic of Korea

⁸Samsung Genome Institute, Samsung Medical Center, Gangnam-gu, Republic of Korea

⁹Department of Intelligent Precision Healthcare Convergence, Sungkyunkwan University, Suwon, Republic of Korea

Contributors MK: conceptualization, writing-original draft, data curation, GK: Conceptualization: MK, STK, and JL. Formal analysis: MK, GK, RK, and K-TK. Methodology: MK, GK, RK, K-TK, JYH, K-MK, WKK, W-YP, and JL. Project administration: STK and JL. Writing—original draft: MK, GK, RK and JL. Acquisition of data and critical revision of the manuscript: MK, GK, RK, K-TK, STK, SS, PGSM, A-BL, II-A, LK, ED, W-YP, and JL. Supervision: JL. JL is responsible for the overall content as guarantor. All authors read and approved the final manuscript.

Funding This paper was supported by SKKU Excellence in Research Award Research Fund, Sungkyunkwan University, 2020.

Competing interests ED, SS, PGSM, A-BL, II-A, and LK are employees and stockholders of AstraZeneca. JL has served a consultant/advisory role in Mirati, Seattle Genetics, and Oncologie. W-YP has equity for Geninus. The other authors declare that they have no conflicts of interest.

Patient consent for publication Not applicable.

Ethics approval The study protocol was approved by the institutional review board (Seoul, Korea; IRB No. 2015-09-053). The study was conducted in accordance with the Good Clinical Practice Guidelines and Declaration of Helsinki. Written informed consent was obtained from all patients.

Provenance and peer review Not commissioned; externally peer reviewed.

Data availability statement Data are available on reasonable request. All raw sequencing data were deposited in the European Nucleotide Archive (ENA) (accession number: PRJEB43396).

Supplemental material This content has been supplied by the author(s). It has not been vetted by BMJ Publishing Group Limited (BMJ) and may not have been peer-reviewed. Any opinions or recommendations discussed are solely those of the author(s) and are not endorsed by BMJ. BMJ disclaims all liability and responsibility arising from any reliance placed on the content. Where the content includes any translated material, BMJ does not warrant the accuracy and reliability of the translations (including but not limited to local regulations, clinical guidelines, terminology, drug names and drug dosages), and is not responsible for any error and/or omissions arising from translation and adaptation or otherwise.

Open access This is an open access article distributed in accordance with the Creative Commons Attribution Non Commercial (CC BY-NC 4.0) license, which permits others to distribute, remix, adapt, build upon this work non-commercially, and license their derivative works on different terms, provided the original work is properly cited, appropriate credit is given, any changes made indicated, and the use is non-commercial. See <http://creativecommons.org/licenses/by-nc/4.0/>.

ORCID iD

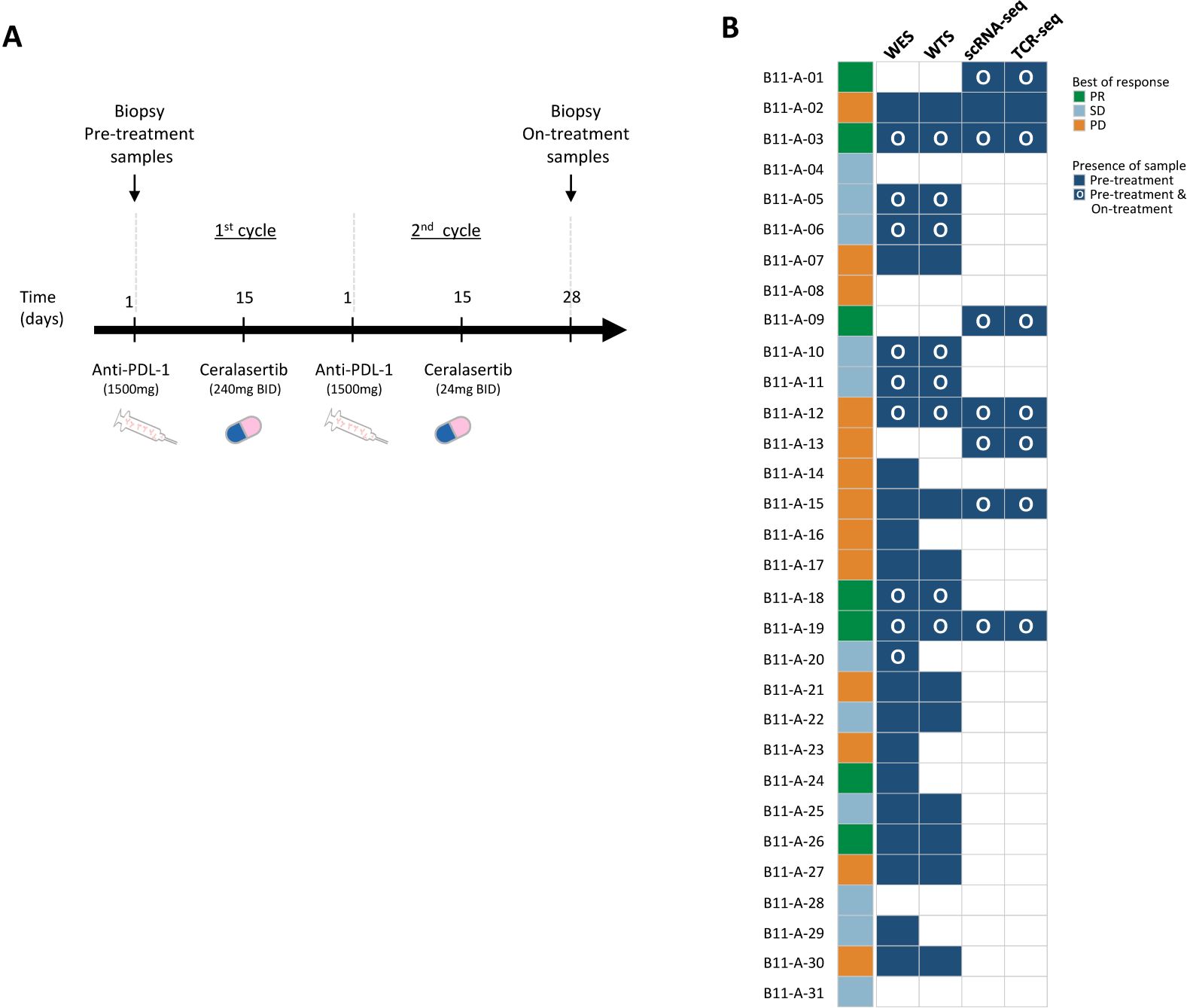
Kyoung-Mee Kim <http://orcid.org/0000-0002-1162-9205>

REFERENCES

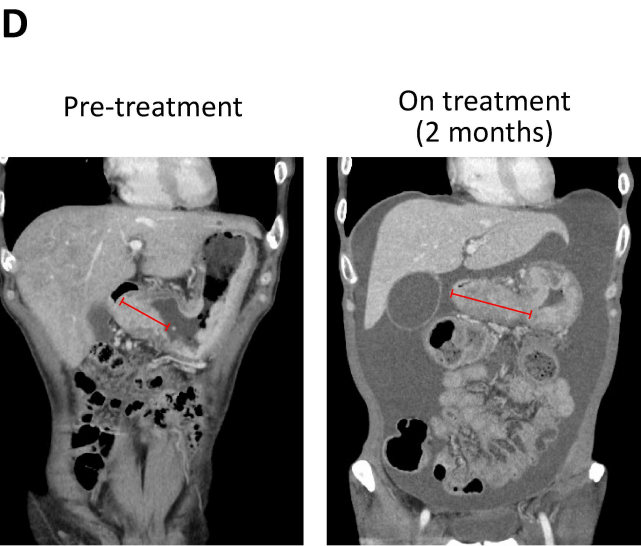
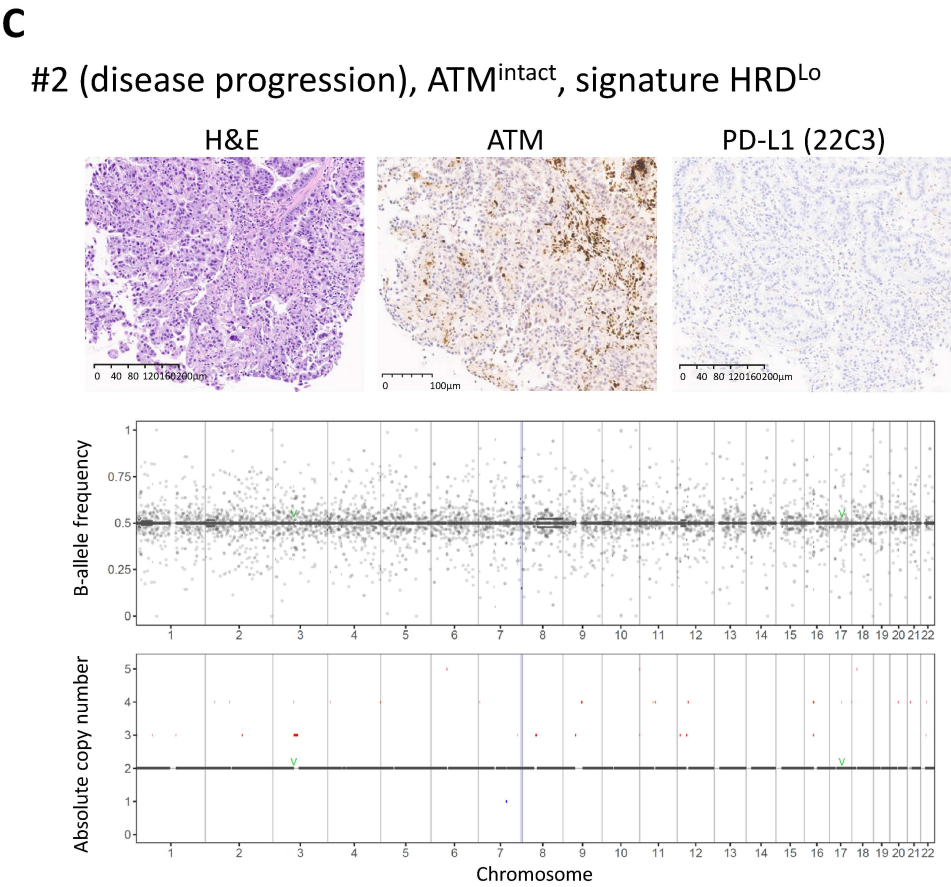
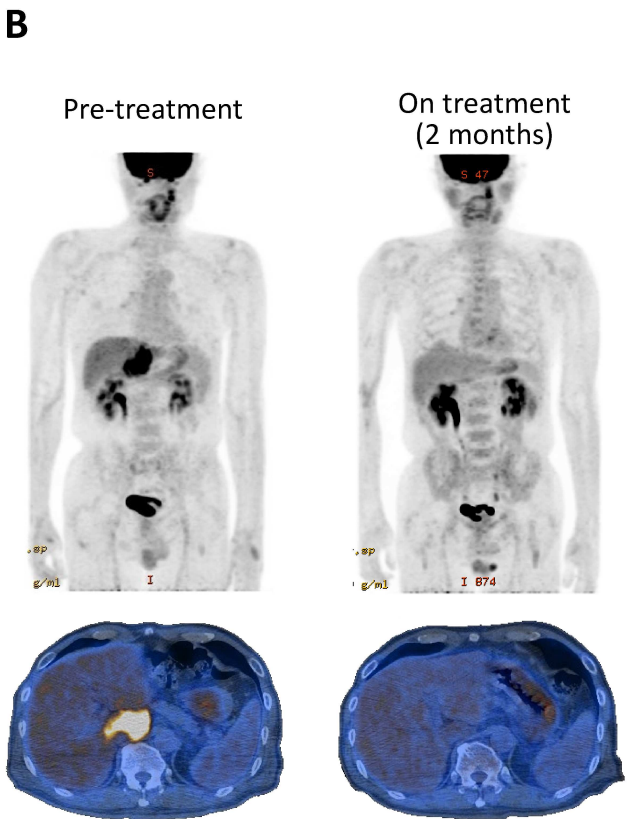
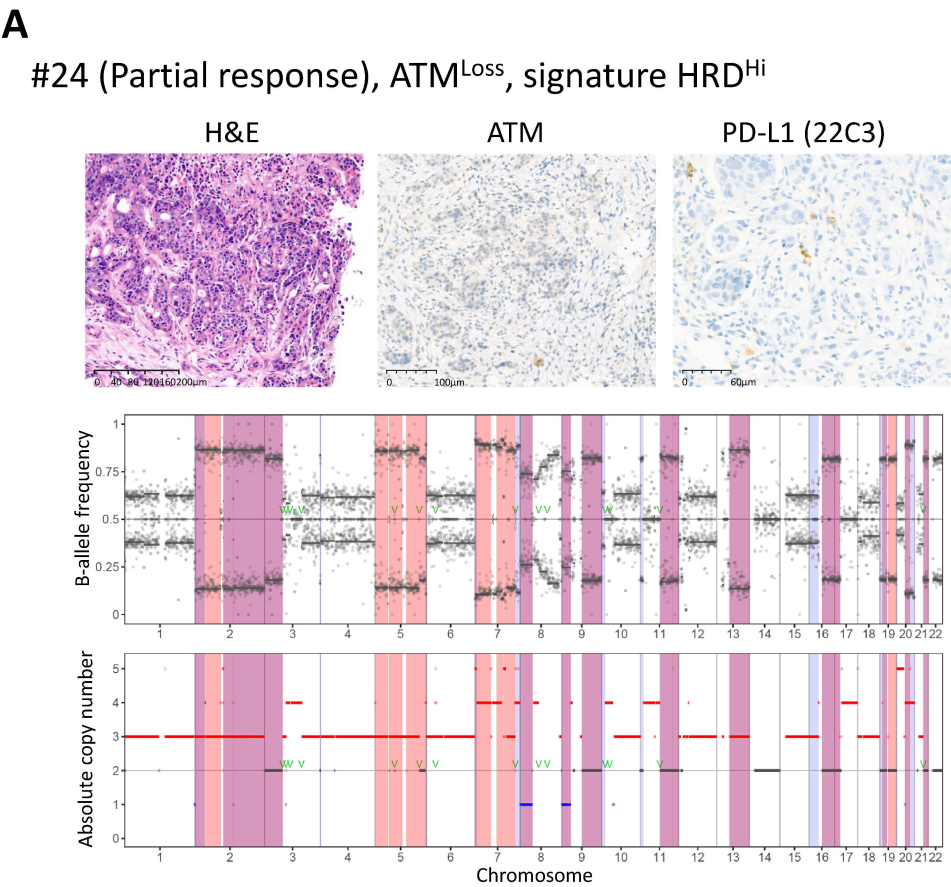
- Kang Y-K, Boku N, Satoh T, *et al.* Nivolumab in patients with advanced gastric or gastro-oesophageal junction cancer refractory to, or intolerant of, at least two previous chemotherapy regimens (ONO-4538-12, ATTRACTION-2): a randomised, double-blind, placebo-controlled, phase 3 trial. *Lancet* 2017;390:2461–71.
- Janjigian YY, Shitara K, Moehler M, *et al.* First-line nivolumab plus chemotherapy versus chemotherapy alone for advanced gastric, gastro-oesophageal junction, and oesophageal adenocarcinoma (CheckMate 649): a randomised, open-label, phase 3 trial. *Lancet* 2021;398:27–40.
- Chung HC, Bang Y-J, S Fuchs C, *et al.* First-line pembrolizumab/placebo plus trastuzumab and chemotherapy in HER2-positive advanced gastric cancer: KEYNOTE-811. *Future Oncol* 2021;17:491–501.
- Tabernero J, Bang Y-J, Van Cutsem E, *et al.* Pembrolizumab plus chemotherapy for previously untreated, HER2-negative unresectable or metastatic advanced gastric or gastroesophageal junction (G/GEJ) adenocarcinoma: KEYNOTE-859. *J Clin Oncol* 2021;39:TPS263.
- Kim ST, Cristescu R, Bass AJ, *et al.* Comprehensive molecular characterization of clinical responses to PD-1 inhibition in metastatic gastric cancer. *Nat Med* 2018;24:1449–58.
- Baxter MA, Middleton F, Cagney HP, *et al.* Resistance to immune checkpoint inhibitors in advanced gastro-oesophageal cancers. *Br J Cancer* 2021;125:1068–79.
- Lemery S, Keegan P, Pazdur R. First FDA approval agnostic of cancer site — when a biomarker defines the indication. *N Engl J Med* 2017;377:1409–12.
- Brown JS, Sundar R, Lopez J. Combining DNA damaging therapeutics with immunotherapy: more haste, less speed. *Br J Cancer* 2018;118:312–24.
- Mouw KW, Goldberg MS, Konstantinopoulos PA, *et al.* DNA damage and repair biomarkers of immunotherapy response. *Cancer Discov* 2017;7:675–93.
- Li A, Yi M, Qin S, *et al.* Prospects for combining immune checkpoint blockade with PARP inhibition. *J Hematol Oncol* 2019;12:98.
- Blackford AN, Jackson SP. ATM, ATR, and DNA-PK: the Trinity at the heart of the DNA damage response. *Mol Cell* 2017;66:801–17.
- Dillon MT, Boylan Z, Smith D, *et al.* PATRIOT: a phase I study to assess the tolerability, safety and biological effects of a specific ataxia telangiectasia and Rad3-related (ATR) inhibitor (AZD6738) as a single agent and in combination with palliative radiation therapy in patients with solid tumours. *Clin Transl Radiat Oncol* 2018;12:16–20.
- Kim ST, Smith SA, Mortimer P, *et al.* Phase I study of Ceralasertib (AZD6738), a novel DNA damage repair agent, in combination with weekly paclitaxel in refractory cancer. *Clin Cancer Res* 2021;27:4700–9.

- 14 Besse B, Awad M, Forde P, *et al.* OA07.08 HUDSON: an open-label, multi-drug, biomarker-directed, phase II platform study in patients with NSCLC, who progressed on anti-PD(L)1 therapy. *J Thorac Oncol* 2021;16:S118–9.
- 15 Kim R, Kwon M, An M, *et al.* Phase II study of ceralasertib (AZD6738) in combination with durvalumab in patients with advanced/metastatic melanoma who have failed prior anti-PD-1 therapy. *Ann Oncol* 2022;33:193–203.
- 16 Angell HK, Lee J, Kim K-M, *et al.* PD-L1 and immune infiltrates are differentially expressed in distinct subgroups of gastric cancer. *Oncoimmunology* 2019;8:e1544442.
- 17 Bailey MH, Tokheim C, Porta-Pardo E, *et al.* Comprehensive characterization of cancer driver genes and mutations. *Cell* 2018;173:371–85.
- 18 Volkova NV, Meier B, González-Huici V, *et al.* Mutational signatures are jointly shaped by DNA damage and repair. *Nat Commun* 2020;11:2169.
- 19 Zhang J-Y, Wang X-M, Xing X, *et al.* Single-cell landscape of immunological responses in patients with COVID-19. *Nat Immunol* 2020;21:1107–18.
- 20 Yost KE, Satpathy AT, Wells DK, *et al.* Clonal replacement of tumor-specific T cells following PD-1 blockade. *Nat Med* 2019;25:1251–9.
- 21 Duhon T, Duhon R, Montler R, *et al.* Co-expression of CD39 and CD103 identifies tumor-reactive CD8 T cells in human solid tumors. *Nat Commun* 2018;9:2724.
- 22 Bagaev A, Kotlov N, Nomie K, *et al.* Conserved pan-cancer microenvironment subtypes predict response to immunotherapy. *Cancer Cell* 2021;39:845–65.
- 23 Kelly RJ, Lee J, Bang Y-J, *et al.* Safety and efficacy of Durvalumab and tremelimumab alone or in combination in patients with advanced gastric and gastroesophageal junction adenocarcinoma. *Clin Cancer Res* 2020;26:846–54.
- 24 Shitara K, Özgüroğlu M, Bang Y-J, *et al.* Pembrolizumab versus paclitaxel for previously treated, advanced gastric or gastro-oesophageal junction cancer (KEYNOTE-061): a randomised, open-label, controlled, phase 3 trial. *Lancet* 2018;392:123–33.
- 25 Shitara K, Van Cutsem E, Bang Y-J, *et al.* Efficacy and safety of pembrolizumab or pembrolizumab plus chemotherapy vs chemotherapy alone for patients with first-line, advanced gastric cancer. *JAMA Oncol* 2020;6:1571–80.
- 26 Klemptner SJ, Bhangoo MS, Luu HY, *et al.* Low ATM expression and progression-free and overall survival in advanced gastric cancer patients treated with first-line XELOX chemotherapy. *J Gastrointest Oncol* 2018;9:1198–206.
- 27 Kim HS, Kim MA, Hodgson D, *et al.* Concordance of ATM (ataxia telangiectasia mutated) immunohistochemistry between biopsy or metastatic tumor samples and primary tumors in gastric cancer patients. *Pathobiology* 2013;80:127–37.
- 28 Brown JS, O’Carrigan B, Jackson SP, *et al.* Targeting DNA repair in cancer: beyond PARP inhibitors. *Cancer Discov* 2017;7:20–37.
- 29 González-Martín A, Pothuri B, Vergote I. Niraparib in patients with newly diagnosed advanced ovarian cancer. *New England Journal of medicine*. *New Eng J Med* 2019;381:2391–402.
- 30 Coleman RL, Oza AM, Lorusso D, *et al.* Rucaparib maintenance treatment for recurrent ovarian carcinoma after response to platinum therapy (ARIEL3): a randomised, double-blind, placebo-controlled, phase 3 trial. *Lancet* 2017;390:1949–61.
- 31 Wright WD, Shah SS, Heyer W-D. Homologous recombination and the repair of DNA double-strand breaks. *J Biol Chem* 2018;293:10524–35.
- 32 Alexandrov LB, Nik-Zainal S, Wedge DC, *et al.* Signatures of mutational processes in human cancer. *Nature* 2013;500:415–21.
- 33 Polak P, Kim J, Braunstein LZ, *et al.* A mutational signature reveals alterations underlying deficient homologous recombination repair in breast cancer. *Nat Genet* 2017;49:1476–86.
- 34 Kwon J, Bakhom SF. The cytosolic DNA-sensing cGAS–STING pathway in cancer. *Cancer Discov* 2020;10:26–39.
- 35 Zhang S, Yuan Y, Hao D. A genomic instability score in discriminating nonequivalent outcomes of BRCA1/2 mutations and in predicting outcomes of ovarian cancer treated with platinum-based chemotherapy. *PLoS One* 2014;9:e113169.
- 36 Zhao EY, Shen Y, Pleasance E, *et al.* Homologous recombination deficiency and platinum-based therapy outcomes in advanced breast cancer. *Clin Cancer Res* 2017;23:7521–30.
- 37 Davies H, Glodzik D, Morganella S, *et al.* HRDetect is a predictor of BRCA1 and BRCA2 deficiency based on mutational signatures. *Nat Med* 2017;23:517–25. doi:10.1038/nm.4292
- 38 Simoni Y, Becht E, Fehlings M, *et al.* Bystander CD8+ T cells are abundant and phenotypically distinct in human tumour infiltrates. *Nature* 2018;557:575–9.
- 39 Wu TD, Madireddi S, de Almeida PE, *et al.* Peripheral T cell expansion predicts tumour infiltration and clinical response. *Nature* 2020;579:274–8. doi:10.1038/s41586-020-2056-8
- 40 Lanitis E, Dangaj D, Irving M, *et al.* Mechanisms regulating T-cell infiltration and activity in solid tumors. *Ann Oncol* 2017;28:xii18–32.
- 41 The Cancer Genome Atlas Research Network. Comprehensive molecular characterization of gastric adenocarcinoma. *Nature* 2014;513:202–9.
- 42 Huang K-lin, Mashl RJ, Wu Y, *et al.* Pathogenic germline variants in 10,389 adult cancers. *Cell* 2018;173:355–70.
- 43 Springer I, Besser H, Tickotsky-Moskovitz N, *et al.* Prediction of specific TCR-peptide binding from large dictionaries of TCR-peptide pairs. *Front Immunol* 2020;11:1803.

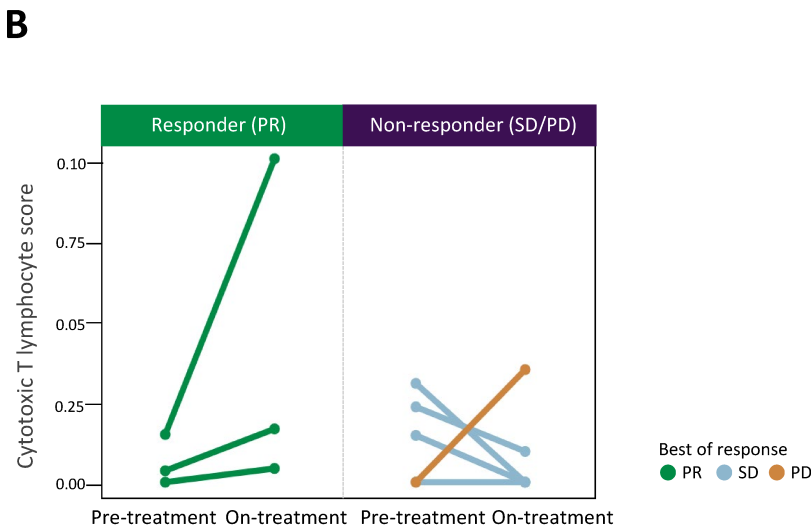
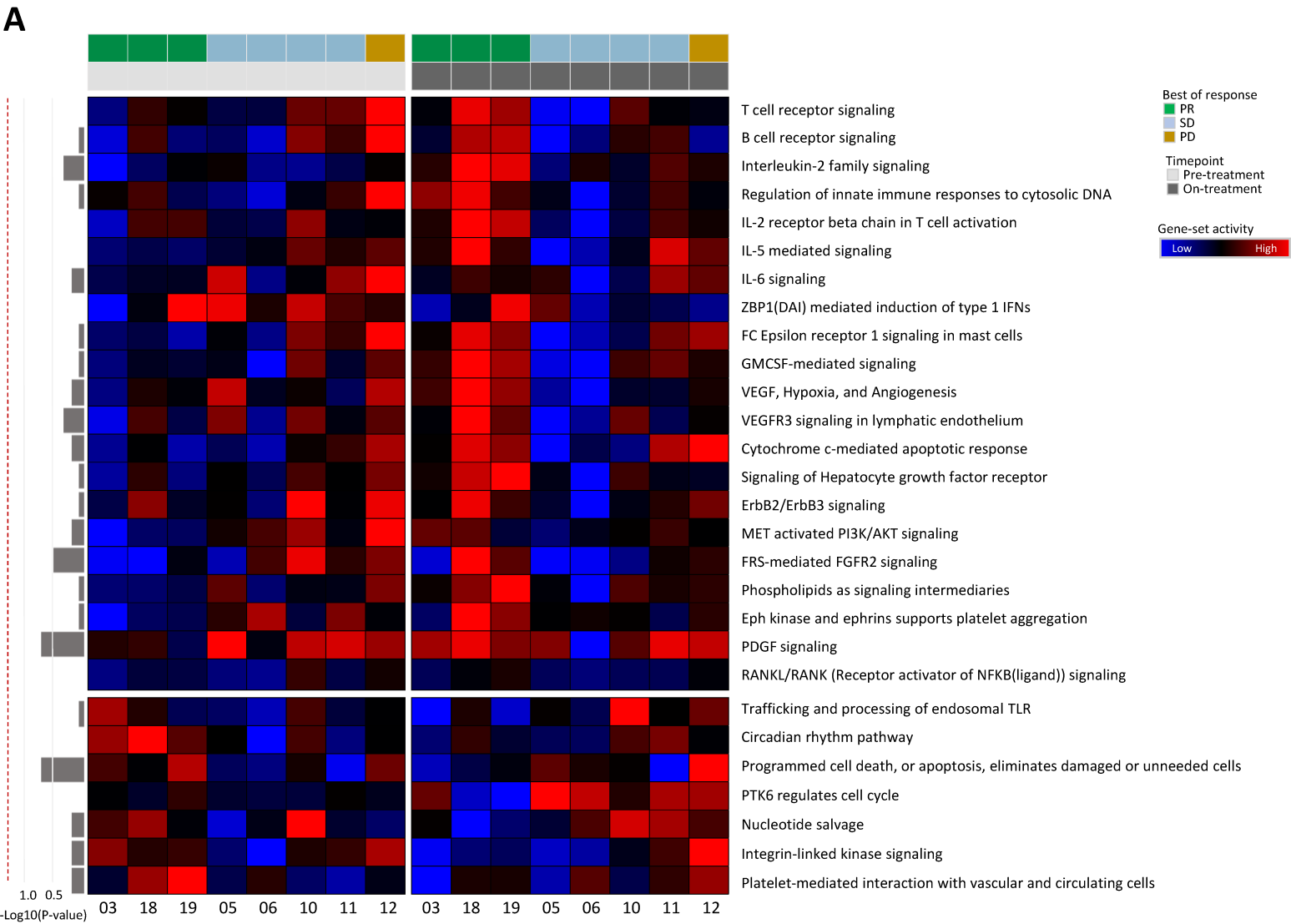
Supplementary figure S1



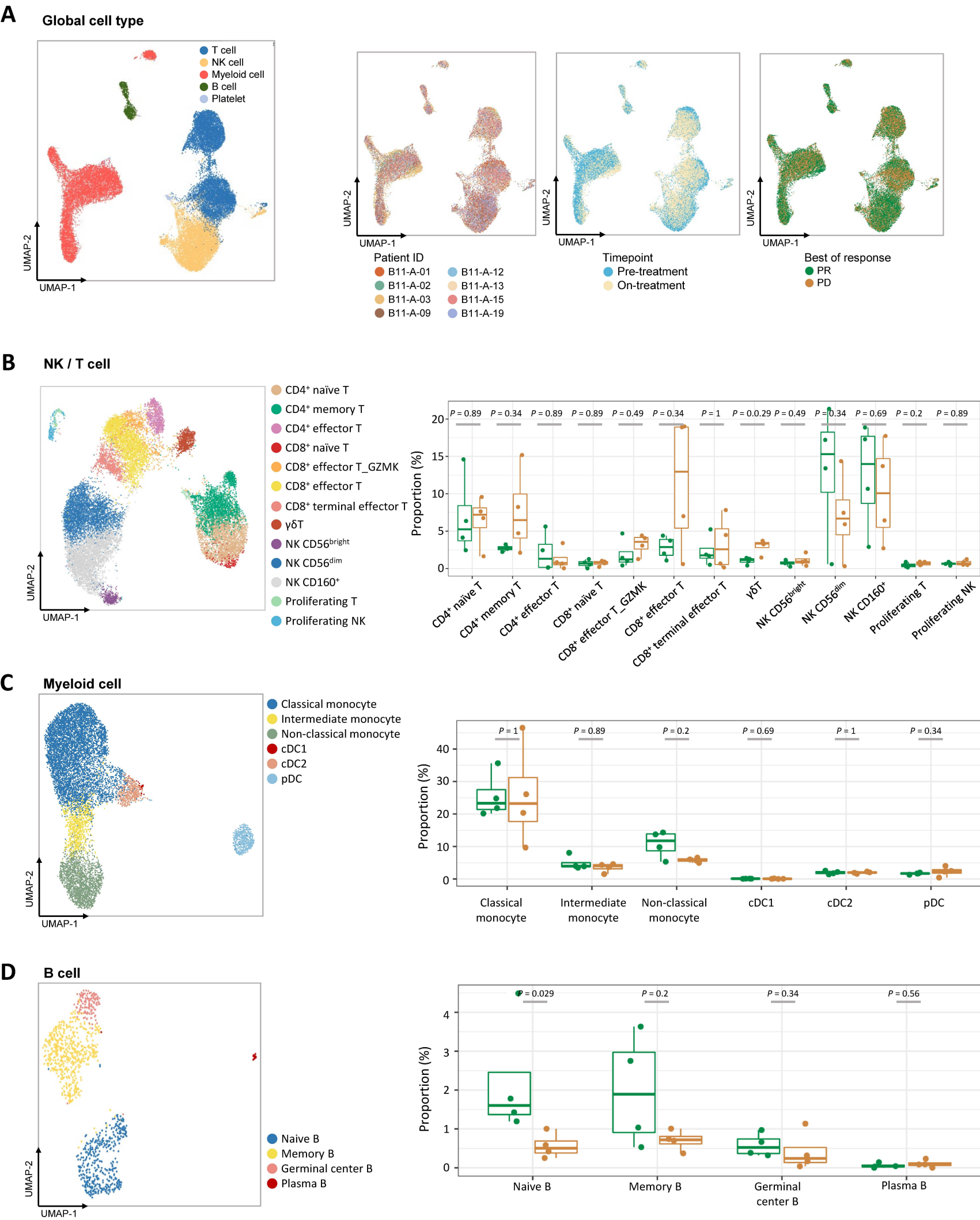
Supplementary figure S2



Supplementary figure S3

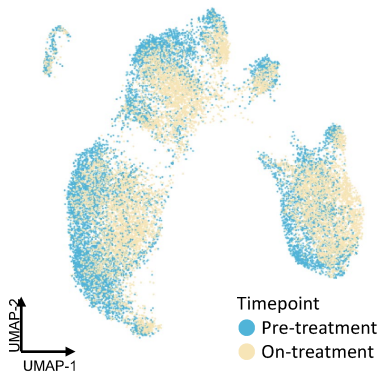


Supplementary figure S4

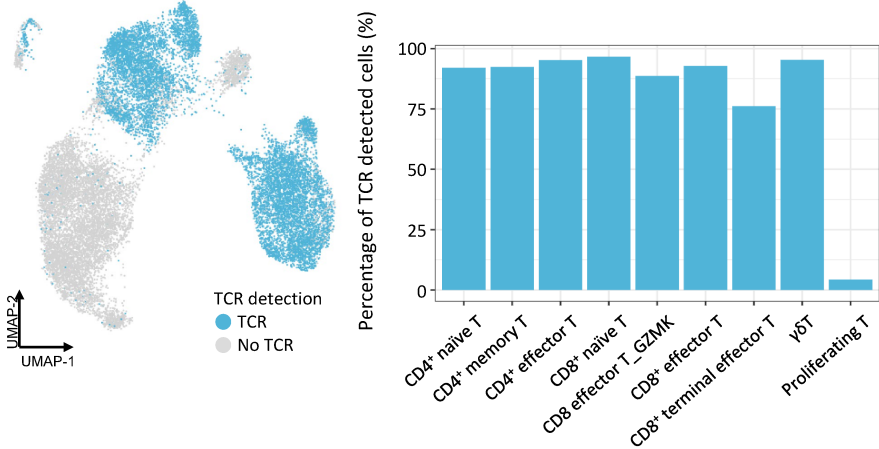


Supplementary figure S5

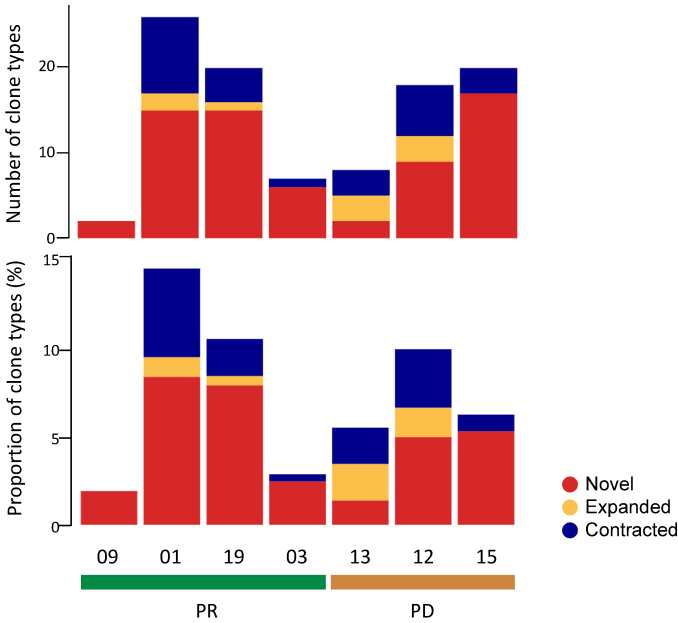
A



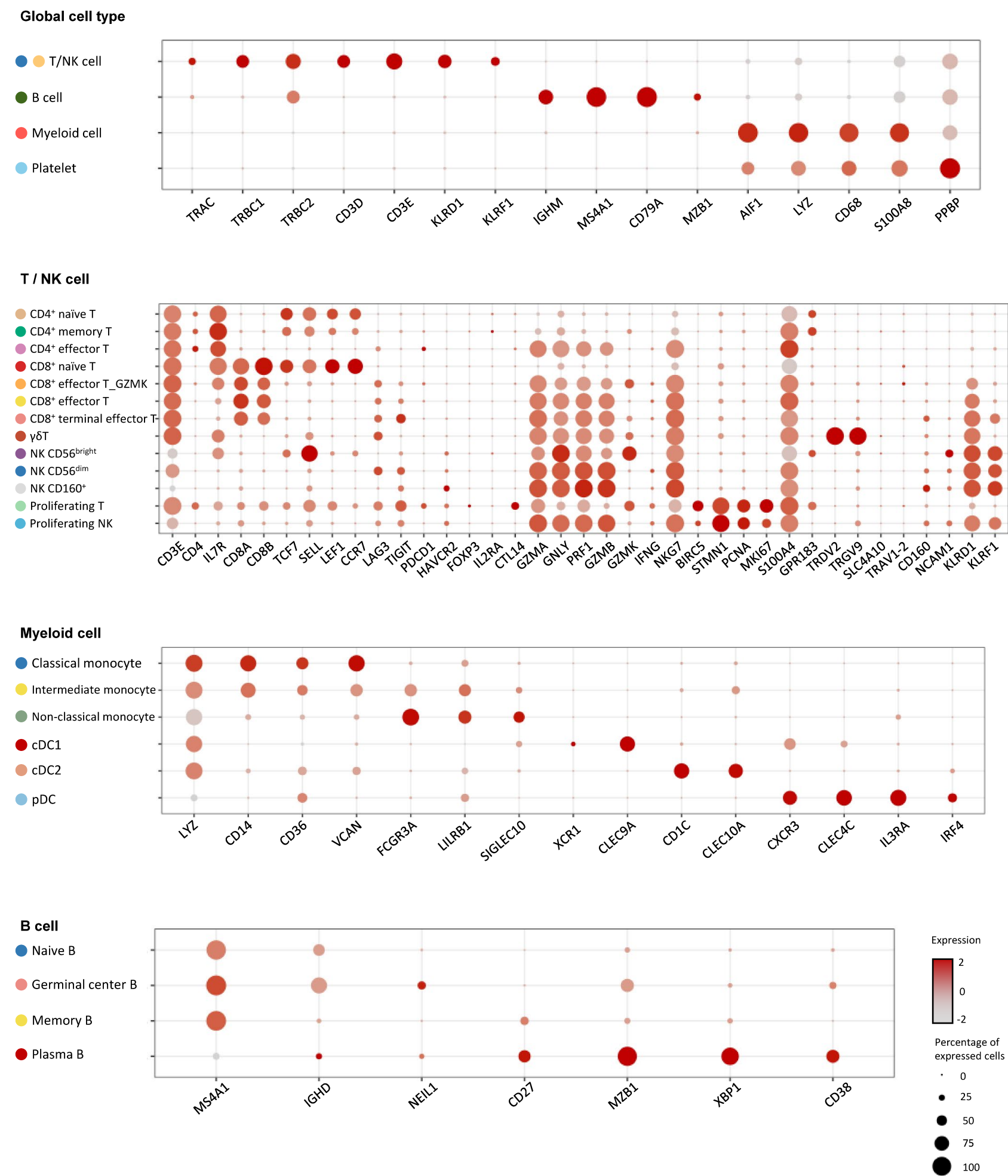
B



C



Supplementary figure S6



SUPPLEMENTARY MATERIALS

Tumor samples and peripheral blood collection

If the tumor content was estimated to be more than 40% after thorough pathological review, tumor DNA was extracted from freshly obtained tissues using a QIAamp Mini Kit (Qiagen, Hilden, Germany) according to the manufacturer's instructions. For DNA analysis, we used RNaseA (cat. #19101; Qiagen). We measured concentrations and 260/280- and 260/230-nm ratios with an ND1000 spectrophotometer (Nanodrop Technologies, Thermo Fisher Scientific, MA, USA) and then further quantified DNA using a Qubit fluorometer (Life Technologies, CA, USA).

Sequencing of Exome and Transcriptome

Genomic DNA from tumor tissue and matched blood samples was extracted using a QIAamp DNA Mini Kit (Qiagen). Library preparation was performed by using the SureSelect XT Human All Exon V6 kit (Agilent). Briefly, 900-1,000 ng of genomic DNA from tumor tissue and matched blood samples was sheared by Covaris Adaptive Focused Acoustics (AFA) sonication device (S2, Covaris Inc.), and 150-200 bp of the DNA fragments were processed for end-repairing, 3'-end adenylation, and ligation to adaptors. Sequencing libraries were performed on the HiSeq 2500 platform (Illumina) in 100-bp paired-end mode of TruSeq Rapid PE Cluster kit and TruSeq Rapid SBS kit (Illumina). RNA sequencing libraries were prepared using TruSeq RNA Exome Library Prep kit (Illumina) according to the manufacturer's protocol. Isolated total RNA was used in a reverse transcription reaction with random primers using SuperScript II reverse transcriptase (Invitrogen) according to manufacturer's protocols. RNA sequencing libraries were prepared via end-repair, 3'-end adenylation, adapter ligation, and amplification and those were sequenced 100-bp paired-end

mode of the TruSeq Rapid PE Cluster Kit and the TruSeq Rapid SBS Kit in Illumina HiSeq 2500 (Illumina).

Variant calling and filtering

Exome sequencing reads were aligned to the human reference genome (GRCh37) using the bwa-mem algorithm from BWA (version 0.7.17). Further pre-processing of read alignment was performed using Genome Analysis Tool Kit (GATK, version 4.1.1.0)[1]. In brief, reads that were marked with duplicates were realigned to indels to remove alignment artifacts, and systematic errors in base quality scores were detected and recalibrated with known polymorphic sites of dbSNP (version 138)[2], 1000G (phase 1)[3] and HapMap (phase 3)[4] data using BaseRecalibrator and ApplyBQSR modules with default option parameters. We sought to identify pathogenic germline variants by scanning BAM files of each tumor and matched normal sample with the list for genomic regions of oncogenic germline variants found across pan-cancer[5]. The extraction of somatic mutations in the tumor samples was carried out with their matched normal samples using Mutect2[6] and Strelka2[7] to establish the highly sensitive somatic variant union sets. Variants with minimum depth ≥ 5 with at least 2 alternative alleles were used for further analysis, and annotated using Ensemble Variant Effect Predictor (VEP)[8] with the GRCh37 database. Allele-specific copy-number was quantified using FACETS (version 0.6.0)[9] in default option parameters, and the resulting copy-ratio profiles were then used to estimate the fraction of cancer nuclei, average cancer genome ploidy, and somatic copy-number alterations by running ABSOLUTE (version 1.0.6)[10].

Mutational signature analysis

To assign single base substitutions (SBS) to the mutational signatures as defined by Alexandrov et al. [11], we utilized the deconstructSigs package (version 1.6.0) [12]. We

considered the characteristic patterns of mutations in trinucleotide context per sample with the reference of ‘signatures.exome.cosmic.v3.may2019’, and the contribution of each biological phenotype was represented as follows: age (SBS1 and SBS5), APOBEC (apolipoprotein B mRNA editing enzyme, catalytic polypeptide-like; SBS2 and SBS13), UV (ultraviolet; SBS7a, SBS7b, SBS7c, and SBS7d), smoking (SBS4), immunoglobulin gene hypermutation (SBS9), HRD (homologous recombination deficiency; SBS3), MMRD (mismatch repair deficiency; SBS6, SBS15, SBS20 and SBS26), NERD (nucleotide excision repair deficiency; SBS8) [13], DPD (DNA proofreading deficiency; SBS10a and SBS10b) and BERD (base excision repair deficiency; SBS18).

Detection of LOH, TAI and LST

In search of additional genetic variants that are associated with HRD, we examined three independent measures of genomic instability: loss-of-heterozygosity (LOH) [14], telomeric allelic imbalance (TAI) [15], and large-scale state transitions (LST) [16]. From allele-specific copy number profiles, we determined LOH when absolute minor allelic copy number was zero and the other allele had absolute copy number > 0 spanning genomic regions over 15 megabases (Mb). LST was regarded in each chromosome when chromosome breaks (translocations, inversions or deletions) in adjacent segments of DNA was observed in larger than 10 Mb. TAI was defined when the absolute copy numbers between minor and major alleles were differentially observed in extending to the telomeric end, and not in crossing the centromere.

Identification of putative neoantigens

We identified putative neo-peptides using Mupexi[17] with NetMHCpan (version 4.0)[18] binding strength predictor between peptides and MHC molecules. The prediction depended on somatic mutations and HLA types. Transcript expression file was used to consider

expression of mutated peptides, which was optional. We performed HLA typing to determine HLA alleles and corresponding MHC complexes using Optitype[19]. We considered the neo-peptides with mutRANK < 2% for further analysis. We regarded a somatic mutation generating at least one neo-peptide as a neoantigen. Based on the cancer cell fraction (CCF) estimated by ABSOLUTE[10], newly emerged neoantigens were defined when the CCF of pre-treatment was zero and the CCF of on-treatment was not equal to zero.

Transcriptome sequencing analysis

Transcriptome reads were aligned to the human reference genome (GRCh38) using the 2-pass default mode of STAR (version 2.6.1)[20] with the annotation of ENSEMBL (version 98). Gene expression abundance as the unit of TPM (transcript per million) was estimated using the default option parameters in running RSEM (version 1.3.1)[21]. We estimated the gene-set enrichment scores of representative pathways involved in the TME using single-sample gene set enrichment analysis (ssGSEA) algorithm for each sample[22, 23]. By integrating the transcriptomic data, we classified each tumor sample into four distinct microenvironment subtypes: immune-depleted, fibrotic, immune-enriched, and immune-enriched/fibrotic[23]. We performed differentially expressed gene (DEG) analysis using the edgeR package[24]. Following normalization using trimmed mean of M values, tagwise dispersions were estimated and subjected to an exact test. DEGs were filtered according to the following criteria: expression fold change > 1.5; and *P* value from Wilcoxon rank sum test < 0.05. We calculated single-sample GSEA (ssGSEA) scores for MSigDB[25, 26] curated canonical genesets (C2.CP) using GSVA software package[27]. The change in ssGSEA scores after treatment was defined as the scores of pre-treatment subtracted from the scores of on-treatment. Intratumoral cell populations were estimated with MCP-Counter[28].

Sequencing of Single-cell RNA and T-cell receptor in peripheral blood mononuclear cells

Peripheral blood mononuclear cells (PBMCs) were isolated by Ficoll (GE Healthcare, Little Chalfont 17-5442-02 UK). After processing, PBMCs were resuspended in freezing media (RecoveryTM cell culture freezing medium, Gibco) and stored in liquid nitrogen. The cells were then cryopreserved in liquid nitrogen until use. All samples showed a viability of around 90% on average after thawing. Single-cell RNA-seq libraries were prepared by using the Chromium Next GEM Single Cell 5' Kit v1.1 (10× Genomics, Pleasanton, CA, USA) following the manufacturer's instructions. Briefly, the Chromium Controller instrument was utilized to encapsulate single cells into droplets and the single cells were barcoded reverse transcription (RT) of mRNA, followed by amplification, shearing and Illumina library construction. cDNA library quality was determined using Agilent Bioanalyzer and Next generation sequencing was performed by using the Novaseq6000 (200 cycles) cartridges from Illumina. TCR V(D)J segments were enriched from amplified cDNA from 5' libraries via PCR amplification using a Chromium Single-Cell V(D)J Enrichment kit according to the manufacturer's protocol (10X Genomics).

Single cell RNA and TCR sequencing analysis

Single cell RNA sequencing (scRNA-seq) reads were aligned to the GRCh38 reference genome and quantified using Cell-Ranger (10X Genomics, version 3.1.0). We filtered out cells which met either of the following conditions: 1) putative doublets predicted by Scrublet[29], 2) low number of detected genes (< 200), and 3) high fraction of mitochondrial contamination (>10%). The remaining cells of raw UMI counts were then log-normalized with the scale factor of 10,000 and scaled across the given samples using Seurat package[30]. We performed the principal component analysis (PCA) on the integrated gene expression

profiles with the most variable 2500 genes, and the top principal components determined by ‘elbow’ heuristics were applied to remove batch effects across samples using Harmony algorithm[31]. For exploratory visualization, cells were projected into two-dimensional Uniform Manifold Approximation and Projection (UMAP) space[32]. Cells were clustered using FindNeighbors and FindCluster functions in Seurat package, and annotated by canonical marker genes.

To process single-cell TCR-sequencing data, we ran CellRanger ‘vdj’ pipeline (10X genomics, version.3.1.0) with the GRCh38 reference for demultiplexing, gene quantification and TCR clonotype assignment. TCR clonality was estimated as follows: [33]

$$Clonality = 1 - \frac{Shannon - Weiner\ index\ (H')}{\ln(\#\ of\ productive\ unique\ sequences)}$$

where Shannon-Wiener index (H') is the measure of diversity. Samples with monoclonal T cell population have a clonality of 0, while the clonality converges to 1 in samples with extremely diverse T cell population. To investigate how T cell clonotypes changed after the treatment, we grouped each T cell clone by comparing the clonal frequency of pre-treatment and that of on-treatment. T cell clones were defined as expanded clones when the clonal frequencies increased significantly compared to those of pre-treatment according to Fisher’s exact test. T cell clones detected only in on-treatment samples were defined as novel clones. We excluded the clones with clone size 1 from the novel clones. We defined the T cell clones exhibiting decreased clonal frequencies as contracted clones based on Fisher’s exact test. The rest of clones are defined as persistent clones.

Prediction of binding affinity of pMHC and TCR

To investigate the binding affinity of novel or expanded CD8⁺ T cell receptors and newly emerged neo-peptides presented by MHC (pMHC), we utilized ERGOII[34], a deep-learning

based tool for prediction of TCR-peptide binding. Inside the tool, long short-term memory (LSTM) neural network model was trained on McPAS-TCR[35], a database of pathology-associated T cell receptor sequences. We calculated the ERGOII binding score for all possible combinations of novel or expanded $CD8^+$ TCRs and pMHCs derived from newly emerged neoantigens, and the highest affinity score for each clone is taken as a representative value for each clone.

1. DePristo MA, Banks E, Poplin R, Garimella KV, Maguire JR, Hartl C, Philippakis AA, del Angel G, Rivas MA, Hanna M *et al.* **A framework for variation discovery and genotyping using next-generation DNA sequencing data.** *Nature Genetics* 2011, **43**(5):491-498.
2. Sherry ST, Ward MH, Kholodov M, Baker J, Phan L, Smigielski EM, Sirotkin K: **dbSNP: the NCBI database of genetic variation.** *Nucleic acids research* 2001, **29**(1):308-311.
3. Genomes Project C, Auton A, Brooks LD, Durbin RM, Garrison EP, Kang HM, Korbel JO, Marchini JL, McCarthy S, McVean GA *et al.* **A global reference for human genetic variation.** *Nature* 2015, **526**(7571):68-74.
4. International HapMap C, Altshuler DM, Gibbs RA, Peltonen L, Altshuler DM, Gibbs RA, Peltonen L, Dermitzakis E, Schaffner SF, Yu F *et al.* **Integrating common and rare genetic variation in diverse human populations.** *Nature* 2010, **467**(7311):52-58.
5. Huang K-I, Mashl RJ, Wu Y, Ritter DI, Wang J, Oh C, Paczkowska M, Reynolds S, Wyczalkowski MA, Oak N *et al.* **Pathogenic Germline Variants in 10,389 Adult Cancers.** *Cell* 2018, **173**(2):355-370.e314.
6. Cibulskis K, Lawrence MS, Carter SL, Sivachenko A, Jaffe D, Sougnez C, Gabriel S, Meyerson M, Lander ES, Getz G: **Sensitive detection of somatic point mutations in impure and heterogeneous cancer samples.** *Nature Biotechnology* 2013, **31**(3):213-219.
7. Kim S, Scheffler K, Halpern AL, Bekritsky MA, Noh E, Källberg M, Chen X, Kim Y, Beyter D, Krusche P *et al.* **Strelka2: fast and accurate calling of germline and somatic variants.** *Nature Methods* 2018, **15**(8):591-594.
8. McLaren W, Gil L, Hunt SE, Riat HS, Ritchie GRS, Thormann A, Flicek P, Cunningham F: **The Ensembl Variant Effect Predictor.** *Genome Biology* 2016, **17**(1):122.
9. Shen R, Seshan VE: **FACETS: allele-specific copy number and clonal heterogeneity analysis tool for high-throughput DNA sequencing.** *Nucleic Acids Research* 2016, **44**(16):e131-e131.

10. Carter SL, Cibulskis K, Helman E, McKenna A, Shen H, Zack T, Laird PW, Onofrio RC, Winckler W, Weir BA *et al*: **Absolute quantification of somatic DNA alterations in human cancer.** *Nature Biotechnology* 2012, **30**(5):413-421.
11. Alexandrov LB, Nik-Zainal S, Wedge DC, Aparicio SA, Behjati S, Biankin AV, Bignell GR, Bolli N, Borg A, Borresen-Dale AL *et al*: **Signatures of mutational processes in human cancer.** *Nature* 2013, **500**(7463):415-421.
12. Rosenthal R, McGranahan N, Herrero J, Taylor BS, Swanton C: **DeconstructSigs: delineating mutational processes in single tumors distinguishes DNA repair deficiencies and patterns of carcinoma evolution.** *Genome Biol*, **17**:31.
13. Jager M, Blokzijl F, Kuijk E, Bertl J, Vougioukalaki M, Janssen R, Besselink N, Boymans S, de Ligt J, Pedersen JS *et al*: **Deficiency of nucleotide excision repair is associated with mutational signature observed in cancer.** *Genome Res* 2019, **29**(7):1067-1077.
14. Abkevich V, Timms KM, Hennessy BT, Potter J, Carey MS, Meyer LA, Smith-McCune K, Broaddus R, Lu KH, Chen J *et al*: **Patterns of genomic loss of heterozygosity predict homologous recombination repair defects in epithelial ovarian cancer.** *British Journal of Cancer* 2012, **107**(10):1776-1782.
15. Birkbak NJ, Wang ZC, Kim J-Y, Eklund AC, Li Q, Tian R, Bowman-Colin C, Li Y, Greene-Colozzi A, Iglehart JD *et al*: **Telomeric Allelic Imbalance Indicates Defective DNA Repair and Sensitivity to DNA-Damaging Agents.** *Cancer Discovery* 2012, **2**(4):366.
16. Popova T, Manié E, Rieunier G, Caux-Moncoutier V, Tirapo C, Dubois T, Delattre O, Sigal-Zafrani B, Bollet M, Longy M *et al*: **Ploidy and Large-Scale Genomic Instability Consistently Identify Basal-like Breast Carcinomas with BRCA1/2; Inactivation.** *Cancer Research* 2012, **72**(21):5454.
17. Bjerregaard A-M, Nielsen M, Hadrup SR, Szallasi Z, Eklund AC: **MuPeXI: prediction of neo-epitopes from tumor sequencing data.** *Cancer Immunology, Immunotherapy* 2017, **66**(9):1123-1130.
18. Jurtz V, Paul S, Andreatta M, Marcatili P, Peters B, Nielsen M: **NetMHCpan-4.0: Improved Peptide-MHC Class I Interaction Predictions Integrating Eluted Ligand and Peptide Binding Affinity Data.** *The Journal of Immunology* 2017, **199**(9):3360.
19. Szolek A, Schubert B, Mohr C, Sturm M, Feldhahn M, Kohlbacher O: **OptiType: precision HLA typing from next-generation sequencing data.** *Bioinformatics* 2014, **30**(23):3310-3316.
20. Dobin A, Davis CA, Schlesinger F, Drenkow J, Zaleski C, Jha S, Batut P, Chaisson M, Gingeras TR: **STAR: ultrafast universal RNA-seq aligner.** *Bioinformatics* 2013, **29**(1):15-21.
21. Li B, Dewey CN: **RSEM: accurate transcript quantification from RNA-Seq data with or without a reference genome.** *BMC Bioinformatics* 2011, **12**(1):323.
22. Barbie DA, Tamayo P, Boehm JS, Kim SY, Moody SE, Dunn IF, Schinzel AC, Sandy P, Meylan E, Scholl C *et al*: **Systematic RNA interference reveals that oncogenic KRAS-driven cancers require TBK1.** *Nature* 2009, **462**(7269):108-112.

23. Bagaev A, Kotlov N, Nomie K, Svelkolkin V, Gafurov A, Isaeva O, Osokin N, Kozlov I, Frenkel F, Gancharova O *et al.* **Conserved pan-cancer microenvironment subtypes predict response to immunotherapy.** *Cancer Cell* 2021, **39**(6):845-865.e847.
24. Robinson MD, McCarthy DJ, Smyth GK: **edgeR: a Bioconductor package for differential expression analysis of digital gene expression data.** *Bioinformatics* 2010, **26**(1):139-140.
25. Subramanian A, Tamayo P, Mootha VK, Mukherjee S, Ebert BL, Gillette MA, Paulovich A, Pomeroy SL, Golub TR, Lander ES *et al.* **Gene set enrichment analysis: A knowledge-based approach for interpreting genome-wide expression profiles.** *Proceedings of the National Academy of Sciences* 2005, **102**(43):15545.
26. Liberzon A, Subramanian A, Pinchback R, Thorvaldsdóttir H, Tamayo P, Mesirov JP: **Molecular signatures database (MSigDB) 3.0.** *Bioinformatics* 2011, **27**(12):1739-1740.
27. Hänzelmann S, Castelo R, Guinney J: **GSVA: gene set variation analysis for microarray and RNA-Seq data.** *BMC Bioinformatics* 2013, **14**(1):7.
28. Becht E, Giraldo NA, Lacroix L, Buttard B, Elarouci N, Petitprez F, Selves J, Laurent-Puig P, Sautès-Fridman C, Fridman WH *et al.* **Estimating the population abundance of tissue-infiltrating immune and stromal cell populations using gene expression.** *Genome Biology* 2016, **17**(1):218.
29. Wolock SL, Lopez R, Klein AM: **Scrublet: Computational Identification of Cell Doublets in Single-Cell Transcriptomic Data.** (2405-4720 (Electronic)).
30. Hao Y, Hao S, Andersen-Nissen E, Mauck WM, Zheng S, Butler A, Lee MJ, Wilk AJ, Darby C, Zagar M *et al.* **Integrated analysis of multimodal single-cell data.** *bioRxiv* 2020:2020.2010.2012.335331.
31. Korsunsky I, Millard N, Fan J, Slowikowski K, Zhang F, Wei K, Baglaenko Y, Brenner M, Loh P-r, Raychaudhuri S: **Fast, sensitive and accurate integration of single-cell data with Harmony.** *Nature Methods* 2019, **16**(12):1289-1296.
32. Becht E, McInnes L, Healy J, Dutertre C-A, Kwok IWH, Ng LG, Ginhoux F, Newell EW: **Dimensionality reduction for visualizing single-cell data using UMAP.** *Nature Biotechnology* 2019, **37**(1):38-44.
33. Cooper ZA, Frederick DT, Juneja VR, Sullivan RJ, Lawrence DP, Piris A, Sharpe AH, Fisher DE, Flaherty KT, Wargo JA: **BRAF inhibition is associated with increased clonality in tumor-infiltrating lymphocytes.** *Oncotarget* 2013, **2**(10):e26615.
34. Springer I, Besser H, Tickotsky-Moskovitz N, Dvorkin S, Louzoun Y: **Prediction of Specific TCR-Peptide Binding From Large Dictionaries of TCR-Peptide Pairs.** *Front Immunol* 2020, **11**:1803-1803.
35. Tickotsky N, Sagiv T, Prilusky J, Shifrut E, Friedman N: **McPAS-TCR: a manually curated catalogue of pathology-associated T cell receptor sequences.** *Bioinformatics* 2017, **33**(18):2924-2929.

Supplementary Figure S1. Study design and sample status (a) Overview of study design and sample collection. (b) Status of samples by data type. Blue filled squares indicate the presence of pre-treatment sample, and blue filled squares with “o” mark indicate the presence of both pre-treatment samples and on-treatment samples.

Supplementary Figure S2. Representative patients with distinct genetic profiles and their responses to ceralasertib in combination with durvalumab.

(a) (Upper) The representative microscopic findings represent ATM complete loss and PD-L1 CPS score 1. (lower) Allele frequency plot demonstrates frequent loss of heterozygosity (LOH, red color), telomeric allelic imbalance (TAI, blue color), and large-scale transition (green checks). Areas colored purple represents both LOH and TAI. Plot showing absolute copy number marks copy number of minor allele (grey line) and total copy number (both major and minor allele). Amplified copy number lined in red and deleted copy number lined in blue. (b) Pre-treatment and on-treatment images of positron emission tomography–computed tomography. (c) (Upper) The representative microscopic findings represent intact ATM expression in tumor nucleus and PD-L1 CPS score 1. (lower) Allele frequency plot demonstrates no apparent LOH. (d) Pre-treatment and on-treatment coronal reconstructed images of computed tomography.

Supplementary Figure S3. Transcriptomic changes in TME signatures and cell types during treatment (a) Heatmap illustrating original GSVA scores of the gene sets shown in Figure 3b. The left dark grey bars represent log-transformed *P* value calculated by comparing GSVA score of responders (PR) and that of progressors (SD,

PD) in pre-treatment samples. **(b)** Changes in cytotoxic lymphocyte abundance during the study treatment. The cytotoxic lymphocyte score was estimated by deconvoluting the WTS data from pre- and on-treatment samples of eight patients.

Supplementary Figure S4. Cell type identification and comparison of the

proportion of each cell type (a) UMAP plot of 32,787 total cells derived from pre-treatment (n=8) and on-treatment (n=7) peripheral blood samples and color-coded by global cell types, sample origin, timepoint, and best response. **(b)** (Left) UMAP plot of 19,621 T/NK cells color-coded by more subdivided cell type. (right) Comparison of the proportion of each subtype between pre-treatment samples from PR patients (green) and those from PD patients (ocher). **(c)** (Left) UMAP plot of 10,744 myeloid cells color-coded by more subdivided cell type. (right) Comparison of the proportion of each subtype between pre-treatment samples from PR patients (green) and those from PD patients (ocher). **(d)** (Left) UMAP plot of 1,143 B cells color-coded by more subdivided cell type. (right) Comparison of the proportion of each subtype between pre-treatment samples from PR patients (green) and those from PD patients (ocher). Only significant *P* values from Wilcoxon rank sum test are shown.

Supplementary Figure S5. TCR detection rate and distribution of CD8⁺ T cell

clones (a) UMAP plot of 19,621 T / NK cells from pre- (n=8) and on-treatment (n=7) peripheral blood samples. Cells are color-coded according to the timepoint. **(b)** (Left) UMAP plot of T / NK cells color-coded by TCR detection. (right) Bar plot showing the percentage of TCR-detected cells in each T cell subtype. **(c)** (Upper) Number of

each categorized clone type per patient. (lower) Proportion of each categorized clone type among all CD8⁺T cell clones.

Supplementary Figure S6. Expression of canonical markers to assign cell types (a) Dot plot showing expression of marker genes used for global cell type annotation. (b) Dot plot showing expression of marker genes used for T / NK cell subtype annotation. (c) Dot plot showing expression of marker genes used for myeloid cell subtype annotation. (d) Dot plot showing expression of marker genes used for B cell subtype annotation.

Supplementary Table S1. Summary of response and survival data

Variable	Value
complete response	0 (0%)
partial response	7 (22.6%)
stable disease	11 (35.5%)
progressive disease	12 (38.7%)
not evaluable	1 (3.2%)
overall response rate	22.6% (7/31)
disease control rate	58.1% (18/31)
median PFS, months (95% CI)	3.0 (2.1-3.9)
median OS, months (95% CI)	6.7 (3.8-9.6)
median duration of response, months (95% CI)	5.7 (4.9-6.5)

Abbreviations: PFS, progression-free survival; OS, overall survival; CI, confidence interval.

Supplementary Table S2. Overall response rate in subgroups stratified by PD-L1 positivity and ATM expression.

Subgroups	N=31
PD-L1-positive	25.0% (6/24)
PD-L1-negative	20.0% (1/5)
intact ATM	14.3% (3/21)
loss of ATM expression	50.0% (4/8)
PD-L1-positive and loss of ATM expression	57.1% (4/7)

Abbreviations: ATM, Ataxia telangiectasia mutated.